NASA TECHNICAL NOTE

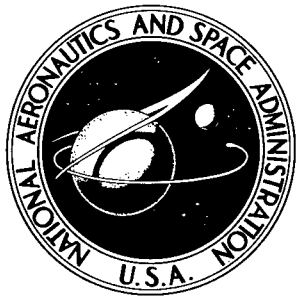

NASA TN D-1866

NASA TN D-1866

DESCRIPTION AND PERFORMANCE OF THREE TRAILBLAZER II REENTRY RESEARCH VEHICLES

by Reginald R. Lundstrom, Allen B. Henning, and W. Ray Hook

Langley Research Center
Langley Station, Hampton, Va.

NATIONAL AERONAUTICS AND SPACE ADMINISTRATION • WASHINGTON, D. C. • DECEMBER 1964

DESCRIPTION AND PERFORMANCE OF THREE TRAILBLAZER II REENTRY RESEARCH VEHICLES

By Reginald R. Lundstrom, Allen B. Henning, and W. Ray Hook

Langley Research Center
Langley Station, Hampton, Va.

NATIONAL AERONAUTICS AND SPACE ADMINISTRATION

For sale by the Office of Technical Services, Department of Commerce, Washington, D.C. 20230 -- Price $1.75

DESCRIPTION AND PERFORMANCE OF THREE TRAILBLAZER II REENTRY RESEARCH VEHICLES

By Reginald R. Lundstrom, Allen B. Henning,
and W. Ray Hook
Langley Research Center

SUMMARY

A description of the Trailblazer II reentry physics research vehicle capable of reentering a 40-pound payload into the atmosphere at 20,000 ft/sec is presented together with the description and results of three flight tests. The vehicle proved to be a workable system during flight tests by accomplishing the objective of reentering a prescribed payload. The dispersion of the impact points of the various stages was within the expected limits except that the first-stage impact was much closer to the launch point than was originally expected. Approximate wobble motions of the spinning body at various times were determined from telemetered quantities. It was possible to determine the chamber pressure time history of the third-stage rocket motor and the thrust time history of the fourth-stage rocket motor from the telemetry carried onboard some of the vehicles. The thrust and pressure curves indicated that the thrust was lower during the first part of the thrust period and higher during the latter part of the thrust period than the values expected for a nonspinning motor.

INTRODUCTION

The physics of bodies reentering the earth's atmosphere at hypersonic speeds is the subject of extensive investigation. It is well known that the reentry causes the air surrounding the body to be heated to a very high temperature. The properties of high-temperature air are known (for example, see refs. 1 and 2), and relatively standard methods are available for computing the temperature and density distributions of the air surrounding the body if the air is in chemical equilibrium. It is suspected that in the case of bodies reentering at speeds of about 20,000 ft/sec and at a near vertical angle, the air surrounding a body and in the wake is not in chemical equilibrium. Also, much remains to be learned about the conditions causing transition from laminar to turbulent flow, particularly in the wake. The dissociation or ionization resulting from this high-temperature air often makes an object appear much larger when viewed by radar than it would appear from ordinary static radar cross-section measurements. This phenomenon is known as radar enhancement. Since the wake is generally very large compared with the body, it is believed to be the major contributor to this radar enhancement phenomenon.

In order to study radar enhancement and other reentry phenomena under conditions that cannot be obtained in laboratory facilities, high-speed reentry into the atmosphere can be obtained by the use of ICBM type vehicles or vehicles which have orbital capabilities. Actually, the use of such large vehicles for reentry study is limited because of the geographical reentry location and high cost. A solid-fuel rocket system, known as Trailblazer, has been designed by the NASA Langley Research Center to perform experimental reentry research by reentering a high-speed test object into the atmosphere near the launch site at a fraction of the cost of ICBM type vehicles. In the case of the vehicles presented herein, which were launched from the NASA Wallops Station, reentering the test object close to the launch site permitted all the ground reentry monitoring instrumentation to be located within 200 miles from the launch site and less than 100 miles from the reentry event.

The Trailblazer program is a cooperative enterprise between the NASA and the Massachusetts Institute of Technology - Lincoln Laboratory to investigate the atmospheric reentry phenomena by using rocket-powered free-flight models. The reentry objects reenter the atmosphere at about 20,000 ft/sec and are tracked with radars and viewed with ground-based optical equipment. The first of these vehicles, called Trailblazer I, is described in reference 3. Because the weight of the reentry object was limited to about 2 pounds, very little weight was available for instrumentation or for heat protection to permit survival to a moderately low altitude. The Trailblazer II is a larger vehicle capable of boosting a 40-pound object to reentry velocities of 20,000 ft/sec. The larger payload weight permits enough heat protection for payload survival below an altitude of 100,000 feet and a significant amount of instrumentation.

Trailblazer II is primarily a four-stage vehicle with the third and fourth stages facing rearward at launch and fired after apogee is reached. This arrangement permits reentry near enough to the launch point so that it may be easily observed with land-based radar and optical equipment. Launchings are made only on very clear nights, when there is no moon, in order to obtain maximum optical coverage.

This report presents a description of the flights of three Trailblazer II test vehicles with different types of payloads. The first, Trailblazer IIa, was instrumented primarily to obtain data on the operation of the vehicle as a system. In this vehicle the fourth-stage motor was an integral part of the payload. Trailblazer IIb used a total of six stages to reenter a small steel pellet at about 40,000 ft/sec. A quite similar experiment performed on a Trailblazer I vehicle is reported in references 4 and 5. The payload of Trailblazer IId was a solid beryllium sphere. The sphere was spring ejected from the fourth-stage motor after the thrust period was completed, and then the expended-fourth-stage motor-case and adapter combination was slowed down with a retro-rocket.

The vehicles were launched at the NASA Wallops Station, Wallops Island, Virginia. Data acquisition and analysis were performed by personnel and equipment of both the NASA and the Lincoln Laboratory.

SYMBOLS

If conversion to the metric system is desired, the following relationships apply: 1 international foot = 0.3048 meter and 1 pound = 0.4536 kilogram.

C_A axial-force coefficient, $\frac{\text{Axial force}}{qS}$

C_l rolling-moment coefficient, $\frac{\text{Rolling moment}}{qSd}$

C_{l_p} damping-in-roll derivative, $\frac{\partial C_l}{\partial\left(\frac{pd}{2V}\right)}$, per radian

C_{l_δ} roll derivative, $\frac{\partial C_l}{\partial \delta}$, per deg

C_m pitching-moment coefficient about center of gravity, $\frac{\text{Pitching moment}}{qSd}$

C_{m_q} damping-in-pitch derivative, $\frac{\partial C_m}{\partial\left(\frac{q'd}{2V}\right)}$, per radian

$C_{m_{\dot{\alpha}}}$ damping due to downwash lag on tail, $\frac{\partial C_m}{\partial\left(\frac{\dot{\alpha}d}{2V}\right)}$, per radian

C_N normal-force coefficient, $\frac{\text{Normal force}}{qS}$

C_{N_α} slope of normal-force-coefficient curve, $\frac{\partial C_N}{\partial \alpha}$, per radian

d reference diameter, ft

I moment of inertia in pitch or yaw, slug-ft^2

I_X moment of inertia in roll, slug-ft^2

M Mach number

p rolling velocity, radians/sec

q dynamic pressure, lb/sq ft

q'	pitching velocity, radians/sec
S	reference area, sq ft
t	time, sec
V	velocity, ft/sec
x_{cp}	vehicle center of pressure, ft from nose
α	angle of attack, radians
γ	flight-path angle, deg
γ_d	angle between flight path of reentering object and plane of outgoing trajectory, positive to right and negative to left of outgoing trajectory
δ	fin deflection, deg
θ	vehicle attitude angle, deg

A dot over a symbol indicates the first derivative with respect to time.

VEHICLE DESCRIPTION AND TESTS

Vehicle Description

Trailblazer II is an unguided solid-fuel rocket system containing four basic stages. As many as two additional stages, depending on payload requirements, have been added. In principle, Trailblazer II is similar to Trailblazer I in that the upper stage motors are enclosed in a structural shell, called the velocity package, and face rearward at launch. The first two stages are used to obtain the desired apogee. The second-stage fins are canted to produce a spin rate of about 10 rps which is sufficient to spin stabilize the vehicle within a small coning angle while above 150,000 feet. At an altitude of about 250,000 feet the velocity package is ejected from the expended second stage with a velocity increment of 8 to 10 ft/sec. This velocity increment results in the expended second stage and the velocity package being separated at apogee by approximately 2,000 to 3,000 feet in slant range from the radars. It was found by experience with Trailblazer I that the chances of radar tracking the unwanted object are minimized if the second stage and velocity package are about 2,500 feet apart when the third stage fires shortly after apogee. The third stage propels the downward-firing stages out of the open end of the velocity-package skin. The firing of the remaining stages drives the payload to its desired reentry velocity. A sketch of the vehicle is shown in figure 1.

Vehicle components.- The first stage consists of a Castor XM33E8 solid-fuel rocket motor capable of producing about 53,000 pounds of thrust for

30 seconds. Attached to the side of the first-stage motor are two Recruit XM19E1 solid-fuel rocket motors, which together produce an additional 60,000 pounds of thrust for about 1.7 seconds. The addition of these assist motors makes it possible to reach a forward velocity of about 500 ft/sec 2 seconds after launch, a fact which markedly decreases the impact dispersion due to winds. The first-stage fins, figure 2, have an exposed area of 12 square feet per panel and are made of cast magnesium with a leading-edge cap of 0.031-inch-thick inconel to protect them from the aerodynamic heating. The fins were bolted to a cast magnesium shroud and, by elongating the bolt holes slightly, it was possible to adjust the incidence of the fin with respect to the motor center line to generally less than 0.05°. The first and second stages are held together with a Marman clamp arrangement containing four explosive bolts. These explosive bolts are ignited by a timer-controlled dual ignition system with timers set for ignition at 35.5 seconds after launch. Ignition of any one of the explosive bolts by either one of the timers is sufficient to release the clamp.

The second-stage rocket motor is a Skat XM45 capable of producing about 45,000 pounds of thrust for approximately 6 seconds. Ignition of the motor is accomplished by the action of a 0.30-second delay squib switch system, which is initiated by the same timer contact that fires the explosive bolts. It was believed that this method of second-stage ignition would provide for a short delay time between first-stage burnout and second-stage ignition but adequate to prevent ignition of the second stage prior to release of the clamp. The second-stage fins have an exposed area of 4 square feet per panel and are made of cast aluminum alloy. Since the aerodynamic heating of the second-stage fins is appreciably more severe than that of the first-stage fins, the leading edge is blunted and made of solid inconel for the first 0.7 inch. Inconel flanges 0.080 inch thick extend back 2 inches from the leading edge. As shown in figure 2 the fin cross section parallel to the rocket center line is a 4° wedge. The fins are bolted to the shroud; in order to roll the vehicle clockwise, as viewed from the rear, the fins on Trailblazers IIa and IIb have a nominal cant angle of 1.50° and those on Trailblazer IId, 1.75°. The holes in the fin root fittings are slotted to permit a possible ±0.67° adjustment about this nominal cant angle, which made it possible to obtain the desired fin setting within ±0.05°.

The velocity-package skin consists of two stainless-steel tubes, a magnesium third-stage separation housing, and a blunted conical nose section made of stainless steel. The connector rings joining these sections together are made of cast magnesium. Inside the velocity package are six equally spaced guide rails (see fig. 1(c)), which run the length of the aft stainless-steel tube and serve as a guide during the exit of the upper stages out the open end of the velocity-package skin. The forward stainless-steel tube contains an inner magnesium tube which serves as a heat shield for the third stage and guides the third stage to the guide rails. The guide rails and tube also add considerably to the stiffness of the unit. Twenty eight $1\frac{1}{2}$-inch-diameter holes, which may be seen in figure 1, are located at the forward end of the velocity package in the magnesium third-stage separation housing to allow the exhaust gases from the burning of the third-stage motor to escape during the time it takes the upper stages to travel the length of the velocity package.

The velocity package is cut off from the remainder of the vehicle 62 seconds after launch by a flexible linear shaped charge placed circumferentially around the velocity-package skin at about station 151. Two circumferential pieces of this shaped charge placed about an inch apart are used. Either of these pieces or sections is capable of severing the velocity package from the rest of the vehicle. Each section of the shaped charge is equipped with its own detonators and ignition system in order to give greater reliability.

At the severed station the velocity-package skin is made of 0.18-inch-thick magnesium and recessed so that the diameter is about an inch less than the diameter ahead of and behind this station. The detonators and shaped charge were placed in this recessed section to prevent the possibility of aerodynamic heating setting off the detonators. The outside of the velocity-package skin was made smooth by covering this recess with a fiber-glass band. The shaped charge was actually bonded to the outside circumference of a heavy 4130 steel ring that fitted closely inside the magnesium casting at about station 151. This wide steel ring served as a mounting plate for the shaped charge and also insured that no metal fragments from the detonation of the shaped charge would injure components inside the velocity package. After the skin has been severed a large bellows assembly pressurized to about 45 lb/sq in. and having a travel of about 1.5 inches separates the velocity package from the expended second stage with a differential velocity of about 8 ft/sec. The bellows and shaped-charge mounting ring remain with the second stage leaving the end of the velocity package open with nothing to obstruct the exit of the downward-firing stages.

The third-stage rocket motor, which fits inside the aforementioned heat-shield tube, is attached to the velocity-package shell with a Marman clamp arrangement. The clamp is released by the axial motion of a push plate actuated by the exhaust blast from third-stage ignition. The third-stage rocket motor is an Altair IX248A10, which produces about 3,000 pounds of thrust for about 39 seconds. This motor, which has a fiber-glass case, was covered with an aluminum-coated tape to improve its radar reflectivity. A sketch of the third stage with various payload mountings is shown in figure 3. Magnesium guide rings are installed at the forward and rearward thrust faces of the rocket case to prevent the fiber-glass rocket case from coming in contact with the guide rails and tube. The motor is ignited after apogee at 330 seconds after launch by a dual ignition system which is activated at velocity-package separation.

The fourth-stage rocket motor is a 15-inch-diameter spherical rocket motor designated Cygnus 15, which was developed at the NASA Langley Research Center. It develops about 5,000 pounds of thrust for 4.8 seconds. The fourth-stage motor is attached to the adapter connecting the third and fourth stages by a diaphragm threaded to the nozzle exit cone; the diaphragm is released by ignition of the fourth stage. Ignition of the fourth-stage motor is accomplished by a dual ignition system at about 308 seconds after velocity-package separation or 370 seconds after launch. In Trailblazer IIa the Cygnus 15 rocket-motor case was part of the payload. In Trailblazers IIb and IId, the fourth-stage rocket-motor case was separated from the payload and reentered separately. Further description of this is given in the section entitled "Payloads."

In Trailblazer IIb a 5-inch-diameter spherical rocket motor designated Cygnus 5 was used as the fifth stage. This motor, also developed at the NASA

Langley Research Center, produces about 530 pounds of thrust for 1.6 seconds. Cygnus 5 was also used as a retro-rocket in Trailblazer IId. Sketches of the reentry stages for the three vehicles are presented in figure 4 and photographs, in figure 5.

Vehicle characteristics.- Weights of the vehicles at various events throughout the flight are presented in table I along with the corresponding center-of-gravity positions and the moments of inertia. The weights listed are measured weights. The combined center-of-gravity positions were calculated from the measured weights and center-of-gravity positions for the separate stages. In most cases the moments of inertia at and after fourth-stage ignition were measured. For events prior to fourth-stage ignition, the moments of inertia are generally estimated.

Aerodynamic parameters for the complete vehicle and for the second-stage and velocity-package combination are listed in table II. The normal-force, axial-force, and pitching-moment coefficients were determined by using the method of reference 6 with slight adjustments made to agree with the measured values of references 7 and 8. Values for C_{l_p} were estimated from the method presented in reference 9, and values of C_{m_q}, from the method described in reference 10.

Spin stabilization.- Sometime after second-stage burnout and about the time of velocity-package separation the vehicle makes the transition from aerodynamic stability to spin stability. The vehicle starts to spin up as soon as the second stage is ignited. As the vehicle spin is increased greater spin stability is effected. At the same time the vehicle is going out of the atmosphere quite rapidly causing the aerodynamic stabilizing moments to decrease quite rapidly. Also, since the vehicle is spun up aerodynamically, by means of canted fins, the rolling moment decreases with the decreasing atmospheric pressure after second-stage burnout and the rolling velocity gradually becomes constant without ever reaching the steady-state value. This may be seen in figure 6 where the calculated missile response to an assumed second-stage thrust misalinement of 0.05° is presented as the variation in pitch attitude angle as a function of time. It may be noted in figure 6 that after about 60 seconds the vehicle attitude angle does not drop off as fast as the flight-path angle because of the spin stability. After the velocity package is ejected at 62 seconds the missile attitude angle remains essentially constant except for the small coning angle. Also shown in figure 6 is the pitch attitude angle of the second stage and velocity-package combination after 62 seconds if velocity-package separation had not occurred. Calculations show that the spin rate is essentially constant above 200,000 feet until the third stage ignites.

An increase in spin rate of about 12 percent would be expected to occur during third-stage burning and of about 25 percent during fourth-stage burning because some of the angular momentum of the burned propellant is transferred to the unburned portion of propellant before leaving the nozzle. The phenomenon is discussed in reference 11 and the estimates of the amount of spin increase were calculated by using methods presented in this reference.

Payloads.- The payloads used in these three vehicles are shown in figures 4 and 5. The payload of Trailblazer IIa (fig. 4(a)), which weighed 45.3 pounds,

had a substructure of magnesium thorium alloy and was covered with an ablating material. The nose section was made of phenolic nylon which was 0.30 inch thick at the stagnation point. The skirt was covered with 0.075-inch-thick epoxy polysulfide. The payload was estimated to survive, for a nominal trajectory, down to an altitude of about 70,000 feet. The overall purposes of the Trailblazer IIa flight test were: (1) to check out the vehicle system, (2) to obtain radar and optical data on the reentry of this particular nose shape, and (3) to obtain some information on the body motions of this vehicle and payload. The vehicle also carried an MIT - Lincoln Laboratory auxiliary experiment which consisted of the lights and the reflector system shown in the back of the payload in figures 4 and 5. This reflector also serves as a telemeter antenna.

The purpose of the flight tests of Trailblazer IIb was to obtain optical data on a small steel pellet of known mass reentering as an artificial meteoroid at a velocity of about 47,000 ft/sec. A total of six stages was used. The fourth-stage rocket motor had a small threaded boss on the front of the case which was used to hold the adapter to support the fifth-stage rocket motor. The final stage was a high-energy accelerator shown in figure 4(b) which was expected to give a velocity increment of 11,000 ft/sec to a steel pellet located in the front of the accelerator. The mass of the 5.8-gram pellet after firing was 2.2 grams ± 0.1 gram as determined by ground tests. The fifth stage and accelerator were very similar to those used for a Trailblazer I test. A more complete description of the accelerator is presented in references 4 and 5.

The purpose of the flight test of Trailblazer IId was to obtain radar and optical data on a solid 8-inch-diameter beryllium sphere weighing 17.8 pounds and reentering at a velocity of about 20,000 ft/sec. The sphere was held in a close-fitting hollow hemispherical cradle by three spring steel straps (fig. 4(c)). These straps were lashed together with a piece of 1/16-inch aircraft cable threaded through two squib-actuated reefing cutters. At the rear of the beryllium sphere was a heavy steel spring having a spring constant of about 50 lb/in. and one end fastened to the adapter. The other end of the spring, when compressed, rested against the rearward part of the sphere. This arrangement was so constructed that ignition of either one of the reefing cutters would cut the aircraft cable and allow the steel straps to be released and the spring to eject the sphere. The result of this action is that the sphere has a velocity 8 to 10 ft/sec greater than the expended fourth-stage rocket case and adapter. The fifth-stage motor was used as a retro-rocket and was rigidly attached to the adapter with the nozzle facing forward; it was ignited about 4 seconds after the ejection of the payload. The firing of this retro-rocket was expected to reduce the velocity of the fourth-stage-case and adapter combination by 1,000 ft/sec, which should have allowed the payload to be about 20,000 feet ahead of the expended rocket case at the onset of reentry. This distance was determined to be sufficient for the radars to track the payload alone during the reentry period. It was believed that the rocket case would become optically visible at a much higher altitude than the payload and also that tip-off forces from the coning motion during retrofiring would displace the objects sufficiently laterally so that the photographed reentry streaks would not appear to be in line or on top of one another from at least one optical station. It was thought that the principal advantages for this arrangement would be that a solid spherical ball could be used which would present the same shape to the free airstream no matter what the orientation of the payload may be, and

that there would be no possibility of contaminating the payload wake by any afterburning of the fifth-stage rocket motor. Aerodynamic-heating calculations made on this payload indicate that it would probably survive to impact. Calculations were also made to see if this payload would be subjected to excessive thermal stress during reentry, which could cause it to break in pieces. The calculations indicated no ill effects would be expected from these thermal stresses.

Vehicle Instrumentation

Trailblazer IIa contained two separate telemetry systems. A telemeter using an FM-FM system and operating on a carrier frequency of 240.2 megacycles was located in the nose section of the velocity package. Its purpose was to provide basic data on the performance of the vehicle during the ascending portion of the trajectory, and the instrument ranges were selected to provide data that could be useful in determining the cause of a vehicle failure if that event should occur. Instruments used for this system were:

Rate gyro (roll)	0 to 13.9 rps
Rate gyro (pitch)	$\pm 100^{\circ}$/sec
Rate gyro (yaw)	$\pm 100^{\circ}$/sec
Accelerometer (X-axis, longitudinal; positive g in direction of first-stage thrust)	35g to -5g
Accelerometer (Y-axis, transverse)	±5g
Accelerometer (Z-axis, normal)	±5g
Magnetic aspect sensor	±600 milligauss
Velocity-package separation switches	0 to 5 volts

The magnetic aspect sensor was installed with its axis 45° to the vehicle longitudinal axis. Its primary function was to provide a backup for the roll-rate gyro as a method for determining roll rate, but it was believed that it might also be useful in determining the approximate magnitude of large coning motions if they should occur. Three microswitches were located 120° apart on the velocity-package separation plane such that they would give an indication when the velocity package separated. If the velocity-package skin was not completely severed by the shaped charge, or if there was any tendency for the velocity package to tilt as it was ejected, one of the switches would operate slightly ahead of the others and it would be noticeable on the telemeter record.

Four steel rods near the nose of the velocity package (fig. 1) were used as the antenna. During the ascending portion of the trajectory an electronic device called a diplexer was used to permit the payload telemeter and the performance telemeter to use the same antenna system without interfering with each other. After third-stage ignition the third- and fourth-stage telemeters utilized music-wire whip antennas which were folded inside the velocity package during the ascending trajectory. A coaxial switch, actuated by the opening of one of the whip antennas, was used to switch from one antenna system to the other.

In Trailblazer IIa a telemeter operating at 244.3 megacycles was located in the nose of the payload. Quantities transmitted were:

Accelerometer (X-axis, longitudinal; negative g in direction of fourth-stage thrust)	100g to -200g
Accelerometer (Y-axis, transverse)	±20g
Accelerometer (Z-axis, normal)	±20g
Rate gyro (pitch)	±400°/sec
Rate gyro (yaw)	±400°/sec
Rate gyro (roll)	0 to 15 rps

One channel measured the forward and reverse transmitter powers by use of a dual directional coupler and a two-segment commutator. The instrument ranges were selected so that they could be useful in determining the cause of a booster failure, if it had occurred, rather than giving an accurate determination of moderate vehicle motions.

Trailblazer IIb also contained two separate telemetry systems. One telemeter located in the nose of the velocity package was identical to that used on Trailblazer IIa. The instruments, instrument ranges, and channel assignments were also the same. In this system two opposing steel rods were used for each of the two antenna systems instead of the diplexer.

The second telemeter, which was located in the adapter connecting the third and fourth stages, was an FM-FM system operating on a carrier frequency of 244.3 megacycles. The primary purpose of this telemeter was to monitor the operation of the third stage. The instruments and ranges were:

Accelerometer (X-axis, longitudinal; negative g in direction of third-stage thrust)	5g to -35g
Pressure transducer	0 to 600 lb/sq in. abs

The pressure transducer measured the pressure inside the chamber of the third-stage motor. Music-wire whip antennas similar to those used on Trailblazer IIa were used after the downward-firing stages had emerged from the velocity-package shell.

Trailblazer IId had three complete telemetry systems. The telemetry system located in the nose of the velocity package was identical to that used for Trailblazers IIa and IIb. The 244.3-megacycle telemeter in the adapter joining the third and fourth stages was similar to that used on Trailblazer IIb except that there were six channels of information instead of two. These were:

Accelerometer (X-axis, longitudinal; negative g in direction of third-stage thrust)	5g to -35g
Pressure transducer (third-stage rocket chamber)	0 to 600 lb/sq in. abs
Accelerometer (Y-axis, transverse)	±5g
Accelerometer (Z-axis, normal)	±5g
Magnetic aspect sensor no. 1	±600 milligauss
Magnetic aspect sensor no. 2	±600 milligauss

The third telemeter had a frequency of 256.2 megacycles and was installed in the adapter between the fourth-stage rocket motor and the payload. Quantities measured were:

Accelerometer (X-axis, longitudinal; negative g in direction of fourth-stage thrust)	5g to -125g
Separation switch system	0 to 5 volts

The main purpose of this telemeter was to monitor the operation of the fourth-stage rocket motor and the payload ejection device. During the upward portion of the flight of Trailblazer IId two opposing steel rods served as the antenna for the 256.2-megacycle telemeter and the other two rods served as the antenna for the 240.2- and 244.3-megacycle telemeters with a diplexer arrangement. A set of music-wire whip antennas in the adapter joining the third and fourth stages and a set in the adapter joining the fourth and fifth stages served as antennas for the 244.3- and 256.2-megacycle telemeters, respectively, after the downward-firing stages had emerged from the velocity-package shell.

The telemetry in all vehicles was built by or under the supervision of MIT - Lincoln Laboratory. Signals were recieved both by MIT - Lincoln Laboratory at their radar site at Arbuckle Neck, Assawoman, Virginia, and by the NASA Wallops Station.

Ground-Based Instrumentation

Instrumentation external to the vehicle was used to determine the vehicle trajectories. Five ground-based radars tracked the vehicle for portions of the flight from launch through reentry. Cameras at various ground stations provided optical tracking during the reentry phase of the payload trajectory.

Radars operated by the NASA Wallops Station and situated in the vicinity of the launching site are the SCR-584, FPS-16, modified SCR-584, and long-range S-band radar. The SCR-584 and the modified SCR-584 (small S-band radars) and the FPS-16 (a C-band radar) are short-range radars and are not capable of tracking the complete trajectory of the Trailblazer vehicles. While tracking the outgoing trajectory these radars assist the long-range S-band radar in acquiring the vehicle through an electronic slaving system. The long-range radar was expected to track the vehicles through their reentry phase and to obtain pertinent data concerning the reentry. Also at Arbuckle Neck, near Wallops Island, MIT - Lincoln Laboratory operated a long-range radar whose transmitting frequencies were in the UHF, S-, and X-band ranges. This radar was expected to track the vehicle from launch through reentry and obtain cross-section and position data from the reentry in these three frequency ranges. Cross-section data from all the MIT radar and from NASA long-range S-band radar are recorded at the MIT site. The MIT - Lincoln Laboratory radar and the NASA long-range S-band radar had the capability of aiding each other in acquiring the object to be tracked.

Reentry tracking is also accomplished by using optical equipment. Ballistic, meteor, and modified aerial cameras are used at various down-range stations. These cameras take photographs of the luminous track that the high-speed payload produces as it reenters the atmosphere. Streak photographs, time-chopped streak photographs, and spectrographs of the visible track taken during reentry provided reentry data.

Prelaunch Tests

In an effort to minimize flight failures many environmental tests were made of various vehicle components. The following prelaunch tests were performed:

(a) Wind-tunnel tests to check estimated aerodynamic parameters for the vehicle are described in references 7 and 8. Wind-tunnel tests were also conducted for the payload of Trailblazer IIa.

(b) Load testing of various fins, shrouds, and adapters was made to insure that they would carry loads that might occur during flight. In order to account for reduced strength during aerodynamic heating, the effect was calculated and a proportionally larger load applied to the nonheated structure.

(c) The natural structural frequencies of the vehicles corresponding to the conditions at second-stage ignition and second-stage burnout were determined experimentally. All payloads and adapters were subjected to accelerations and vibrations corresponding to those that might be encountered during third-stage thrust or the most severe conditions that are expected to be experienced during the flight.

(d) Several tests were performed on the velocity-package separation system. The tests insured that the shaped-charge cut was complete and that the steel mounting ring adequately protected vulnerable parts from flying metal fragments.

(e) Several tests were made to insure that the third and fourth stages emerged properly from the velocity-package skin during third-stage ignition. For these tests the third-stage case was ballasted to the proper weight and fitted with an igniter and a charge whose burning gave the same characteristics as the first half second of third-stage burning. This motor was installed in a velocity package with the mechanical system used in a flight test. The velocity package was placed on a set of rails for testing so that both the velocity-package skin and the third-stage motor would be free to move during the test.

(f) The fourth-stage rocket motor was mounted in a flight test vehicle having about the same weight as the Trailblazer IIa payload. This vehicle was launched while being spun at 11 rps. A second test vehicle was also launched while being spun at about the same rate as Trailblazer IIb. These tests gave good indication that the burning characteristics of this rocket motor would not be adversely affected by the spin rates to be encountered during flight testing. These tests were similar to the test described in reference 11.

(g) The timers of each vehicle were checked to insure that they would not be affected (within ± 1 second) by the vibrations, spin, or accelerations that would be encountered during the flight. Just prior to launch, checks were made on the timers and associated wiring (by using light bulbs instead of rocket igniters) to insure that the times of all the various events were what was desired for the flight.

During assembly, the vehicles were dynamically balanced for the following conditions: second-stage ignition, velocity package alone, third-stage ignition, and fourth-stage ignition. In each case the balanced configuration represented

conditions immediately after a separation. Balancing was performed to bring the center of gravity within about 0.002 inch of the axis of spin for the balancing operation. Runouts, or measurements read with a dial indicator resting against the external contour of the vehicle as the vehicle is very slowly rotated in the spin balancer, were not greater than 0.050 inch for the complete velocity package or 0.020 inch for the loaded-third-stage and payload combination. Balance weights were added to bring the principal axis of the stage being balanced within about 0.005° of the spin axis when the stage was mounted in the balancer.

The second-stage—velocity-package combination was balanced on a horizontal balancing machine whereas the velocity package by itself and smaller sections were balanced on a vertical balancing machine. Photographs of vehicle components in these facilities are shown in figures 7 and 8.

Launch

The launcher for the Trailblazer II vehicles was capable of being elevated from 0° to 89° and pointed through a large range of azimuth angles. It was constructed so that the vehicle was guided during the first 4 inches of travel. A photograph of one of the vehicles mounted on the launcher in launch position is presented in figure 9. Since it was necessary to have the reentry occur close to the down-range camera sites and stay within the range safety regulation, the nominal trajectory chosen had a launch elevation angle of 80° and an azimuth angle of 155°.

The Trailblazer II vehicles had no guidance system with which to assure that the vehicle follows the nominal trajectory; therefore, deviation of the vehicles from the nominal trajectory can only be corrected before the vehicle is launched. This deviation or dispersion is dependent on a number of factors. The factors that were considered in estimating the disperison impact areas included fin misalinement, thrust misalinement, thrust and impulse errors, drag calculation errors, weight variations, and wind. Of these factors, wind, fin misalinement, and thrust misalinement contribute nearly all the errors that cause dispersion. Wind, which is the largest contributor of dispersion, can be conpensated for by measuring the winds prior to launch and adjusting the launcher in elevation and azimuth so that the error in flight path and azimuth angle is within ±1° and ±5°, respectively, during first-stage thrusting. The second largest contributor to the dispersion error at first-stage burnout was expected to be the fin and thrust misalinements. For dispersion calculations the fin and thrust misalinements were assumed to be 0.1° and 0.05°, respectively. Figure 10 shows the estimated impact areas for the expended first stage, the expended second stage and velocity-package shell, and the expended third stage. The third-stage impact area also allows for 5° of tip-off due to wobble and thrust misalinements from the altitude of third-stage ignition. Included in this figure are the actual impact points of the expended stages of Trailblazers IIa, IIb, and IId calculated from their last known position. All the impact points shown here fall within the predicted impact areas. The first stage of Trailblazer IIb was not tracked by radar after its separation from the vehicle so its impact point is unknown.

As was stated previously, wind was the largest contributor to the dispersion; therefore, allowances for wind were made to the launcher setting which would permit the vehicle to obtain the proper flight-path angle and azimuth heading at the end of the first-stage thrusting. The method used for wind compensation is fully described in reference 12. The effect winds have on the vehicle is shown in figure 11 where the variation of altitude with the percent of total change in flight-path angle for a constant wind is illustrated. This curve covers the thrusting period of the first stage from 0 to 83,000 feet. It is shown that 50 percent of the change in flight-path angle due to a constant wind occurs from 0 to 1,000 feet. As explained in reference 12, high-altitude sounding balloons capable of being tracked by radar were used to determine speed and direction of the wind up to 83,000 feet. Low-altitude winds are monitored from a 250-foot-high anemometer tower with measurements taken every 50 feet. The wind velocity and direction data from the balloon runs and the anemometer tower are fed into an electronic computer. Results from the computer give the elevation and azimuth angles at which the launcher is set. Good results from the wind-compensation method are indicated in figure 10 by the two impact points near the center of the second-stage and velocity-package-skin impact areas.

RESULTS OF FLIGHT TESTS

The data obtained from the flight tests of three Trailblazer II vehicles are presented herein as the trajectory, roll rate, body motion, separation, and reentry results. The analysis of the reentry data is beyond the scope of this report, but the data are shown herein as results obtained from the satisfactory operation of the Trailblazer II vehicles.

Trajectory Results

A typical Trailblazer II nominal trajectory for an 80° elevation angle at launch is shown in figure 12 for the three vehicles described herein. The altitude, horizontal range, velocity, flight-path angle, and time for the various events are given in table III for both the nominal, or predicted, trajectory and for the actual flight trajectory where available. With the combined use of the figure and the table an adequate description of the nominal flight trajectory can be obtained. After the first and second stages burn out, the second-stage rocket-motor case and the velocity package coast together until 62 seconds after launch. At this time these two parts are separated at a separation velocity of about 8 to 10 ft/sec so that at 330 seconds the empty rocket-motor case and the velocity package are about 2,500 feet apart. The spin that was generated by the canted second-stage fins maintains the velocity package at an attitude that is approximately equal to the flight-path angle at velocity-package separation. Shortly after apogee when the third stage is ignited, the velocity package is still at the same attitude as it was at 62 seconds, which causes the thrust vector from the third-stage motor to be almost perpendicular to the velocity vector. Thus, the flight path of the reentry stages during third-stage burning turns sharply into an almost vertical direction with respect to the surface of the earth. The expended second-stage rocket-motor case, which follows approximately the same trajectory as the velocity package, continues on its

ballistic trajectory somewhat behind the empty velocity-package shell, and these two parts impact in the same general area.

Also included along with the nominal data in figure 12 and in all the subsequent figures are the actual flight data gathered from telemeter records, radar, and optical tracking stations. A radar track was obtained of the complete first-stage trajectory of Trailblazer IId and is presented in figure 12(c). Preflight calculations indicated that the stability of the expended first stage alone was marginal. Due to the difficulty of estimating the aerodynamic parameters of anything as irregular as the adapter joining the first and second stages, it could easily be that the expended first-stage booster is aerodynamically unstable after being separated from the remainder of the vehicle. The original predicted impact area for the first stage, assuming a stable condition, is illustrated in figure 10 by the small ellipse outlined in dashed lines. The apparent instability of the first stage alone created a high-drag condition and the first stage actually impacted much closer to the launch point. The estimated impact area of figure 10 was moved closer to the launch point after recalculation of the first-stage trajectory. An impact point for Trailblazer IIa estimated from a partial track of the first-stage rocket motor is also shown to be within this new impact area.

The nominal axial acceleration of a typical Trailblazer II flight during the burning of the four primary stages is presented in figure 13. The actual longitudinal acceleration of Trailblazer IId is also presented in this figure. The acceleration of the first and second stages is shown in figure 13(a). It can be seen that for this vehicle the acceleration for both the first and second stages was lower than predicted. Figure 13(b) shows the acceleration of the two reentry stages. The reentry sequence of the test vehicle started about 5 seconds earlier than planned. The shape of the acceleration curve for the fourth stage appears to be changed appreciably from the theoretical curve. This difference is due largely to the shape assumed for the nominal thrust curve. The thrust curve for the fourth stage is presented in figure 14. When the axial-acceleration data were used to calculate an actual thrust curve obtained during the flight, the curve rather closely resembled the thrust curve from a static test corrected to vacuum conditions. The measured chamber pressure for the third-stage motor of Trailblazers IIb and IId is presented in figure 15. The tendency to have a slightly reduced thrust early in the burning period and increased thrust near burnout appears to be typical for motors burning while spinning.

The variation of velocity with time for the outgoing portion of the trajectory is presented in figure 16 and for the reentry portion of each flight in figure 17. Variation of altitude with velocity for the reentry part of each flight is presented in figure 18. The following is a résumé of the flight trajectory of each of the test vehicles.

Trailblazer IIa.- The apogee of the flight trajectory of Trailblazer IIa, shown in figure 12(a), was about 100,000 feet lower than predicted. In spite of the altitude loss, the reentry stages performed satisfactorily and reentered the payload at 19,700 ft/sec and at approximately the predicted horizontal range. The outgoing velocity plot of figure 16 shows the decrease of about 350 ft/sec from the predicted velocity at second-stage burnout. This loss in velocity and,

consequently, the low apogee were attributed to a loss in thrust of the first stage due to the propellant in the rocket motor being at well below normal operating temperatures. For subsequent launchings a heating jacket was provided in order to keep the first-stage motor up to normal temperature. The jacket was removed prior to launch. The predicted reentry velocity of the payload as shown in figures 17(a) and 18(a) was obtained in spite of the loss in outgoing velocity and maximum altitude. Optical data for the payload are presented in figures 17(a) and 18(a). The velocity-altitude plot obtained from optical tracking compares well with the predicted velocity-altitude plot. (See fig. 18(a).)

Trailblazer IIb.- The flight trajectory of Trailblazer IIb, as shown in figure 12(b), was higher than predicted, the apogee being about 1,000,000 feet. This high trajectory was due to the resultant flight-path angle being about $1\frac{1}{2}^{\circ}$ higher than nominal at the end of the first-stage burning. This vehicle obtained the predicted peak velocity on the outgoing part of the trajectory, shown in figure 16, but due to a high trajectory the apogee velocity was lower than predicted. The firing of the reentry stages was satisfactory. The reentry velocity for Trailblazer IIb is presented in figures 17(b) and 18(b). The small pellet was not tracked by radar. The fourth- and fifth-stage rocket motors were tracked by radar and their velocities show good agreement with the predicted velocities until burnout of the fifth stage. The velocity at the end of the fifth-stage burning is 1800 ft/sec lower than predicted. Wobble could have produced this loss in that the thrust vector would not have been in line with the velocity vector. Optical tracking data for the pellet are presented in figures 17(b) and 18(b). Also presented in figure 18(b) are optical-tracking data for the reentry of the third, fourth, and fifth stages. The pellet did not obtain its predicted velocity. According to the optical-tracking data, the pellet did reach a maximum velocity of about 38,900 ft/sec. This velocity is the resultant velocity of the fifth-stage velocity, and the pellet velocity as it was ejected from the accelerator. The optical-tracking data indicated that the angle between the luminous track of the fifth-stage case and the pellet track was about $11\frac{1}{3}^{\circ}$. The velocity of the fifth stage as obtained from optical-data reduction was about 33,800 ft/sec. By using the fifth-stage velocity, the pellet velocity, and the angle between the two it can be determined that the accelerator propelled the pellet at about 8,800 ft/sec at an angle of 60° to the direction of flight. Apparently, a large wobble angle developed during the burning of the fifth stage; it was possibly created by burning through of one side of the nozzle. This wobble angle also could account for the velocity loss of about 1,800 ft/sec in the fifth-stage trajectory. Even though the last two stages had a high spin rate at this time the moment of inertia is so small (table I) that a small disturbing moment could create a wobble of this magnitude.

Trailblazer IId.- The outgoing phase of the trajectory of Trailblazer IId in figure 12(c) followed the predicted path fairly well, but was about 50,000 feet low at apogee. This was probably due to reduced thrust in the second stage. The reentry stages all fired 5 seconds earlier than predicted but worked satisfactorily. The predicted reentry velocity plotted against time and altitude is presented in figures 17(c) and 18(c) and compared with radar tracking data. The velocity of the third stage was about 1,100 ft/sec lower than predicted, which is indicated by the constant lower acceleration produced during

its burning. Therefore, the maximum velocity obtained by the 8-inch spherical solid reentry body is 18,800 ft/sec, which is 1,100 ft/sec lower than the nominal. Optical tracking data for the payload are presented in figures 17(c) and 18(c). Optical tracking data are also presented in figure 18(c) for the third and fourth stages.

Roll Rate Results

The nominal roll rate for each vehicle is presented in figure 19 along with data obtained during the flight of each vehicle. The flight data were obtained from a rate gyro, an aspect magnetometer, and from the telemeter signal strength. The data from the rate gyro are read directly, and the direction of roll can be determined; whereas, the data from the magnetometer and the signal strength are obtained by counting cycles on the telemeter trace. For each cycle on the magnetometer trace there is one complete revolution of the vehicle, whereas for two cycles on the signal-strength trace there is one revolution of the vehicle. The roll rate from the rate gyro and from the signal strength or magnetometer is presented in figure 19 for comparison. These two data-measuring systems agree quite well with one another.

Even though the second-stage fins are canted to produce roll in the vehicle, little or no roll occurs during the first-stage thrust period as the rolling moment due to the downwash effect of the deflected second-stage fins on the first-stage fins is about equal and opposite to the rolling moment of the deflected second-stage fins. This same effect was noted in the case of Trailblazer I. (See ref. 3.) When the second stage is ignited and starts burning the roll rate immediately increases until separation. The roll rate is constant from separation until third-stage ignition. The roll rate was not obtained throughout the complete flight because the payload telemeter failed at fourth-stage ignition on Trailblazer IIa and the final three reentry stages of Trailblazer IIb were not instrumented.

In Trailblazer IIa the roll rate experienced a slight decrease near the end of the third-stage burning at $t = 361$ seconds. At this time a disturbance occurred which was noticeable on the telemeter channels measuring angular rates. The roll rate was decreased slightly and the amplitudes of the pitch- and yaw-rate oscillations were increased, suggesting an increase in the amplitude of the coning angle. The longitudinal acceleration had already started to decrease before 361 seconds showing that the motor thrust was already in the tail-off period. It is believed that a section of the nozzle diffuser may have come off at this time.

Body Motions

A spin-stabilized vehicle that is above the atmosphere will have a tendency to wobble when disturbed by moments caused by the separation of the vehicle parts or a slight asymmetry in the thrust of a rocket motor. Whenever any one of these separations takes place a change in the moment of inertia of the vehicle results. A change in the moment-of-inertia ratio, I/I_X, could be detrimental; if the ratio is close to unity the wobble angle could be increased to

an undesirable magnitude. If the wobble angle is large the dispersion of the reentry payload or object can be quite extensive. During the flight of the Trailblazer vehicles there are times when knowledge of the wobble angle is of special interest. These times are before and after the separation of the velocity package from the empty second-stage rocket motor and before, during, and after the third-stage burning. Wobble-angle data were obtained from the pitch or yaw rate gyros and the normal or transverse accelerometers.

In the case of Trailblazer IIa the telemeter record was of very poor quality, but an attempt was made to extract some numbers from the pitch and yaw gyros in order to obtain an idea of the wobble angles. Before the velocity package separated from the burned-out second stage, the wobble angle was about 6.8° and after separation the angle was about 2.0°. Immediately after third-stage ignition, or approximately 330 seconds, the angle of wobble was about 2.6°; at 340 seconds, 1.9°; and at 360 seconds, 1.6°. At 362 seconds, or shortly after the disturbance that occurred to the vehicle, the wobble angle increased to 7.7°. No data were available after the fourth-stage ignition because of telemetry failure.

For Trailblazer IIb the pitch and yaw rate gyros in the performance telemeter indicated that before velocity-package separation at 62 seconds the wobble angle was about 10.3°. After separation at 63 seconds the wobble angle decreased to about 2.3°. Since the vehicle is out of the sensible atmosphere at this time no change in wobble angle occurred until third-stage ignition. Further information on the wobble angle during reentry was not available.

During the flight of Trailblazer IId the performance telemeter failed at the end of second-stage burning; therefore, no rate measurements were obtained during the desired times. The telemeter in the adapter joining the third and fourth stages recorded accelerations, and it was determined that the normal and transverse accelerometers would be able to record the wobble data if the oscillations were large enough. Since no oscillations were detected on the accelerometer traces, it was calculated that the wobble angle had to be less than 3.7° at 63 seconds, or after velocity-package separation; 0.6° at 321 seconds, or third-stage ignition, and 13.8° at about 365 seconds, or near the end of third-stage burning.

On another Trailblazer II vehicle, not described in this paper, the wobble angle calculated from the pitch and yaw rate gyros was about 7° before separation at 62 seconds and 2.4° after separation at 63 seconds. Also, a calculation made from an accelerometer trace during third-stage burning at 337 seconds indicated that the wobble angle was 5.3°.

Separation Results

The velocity package separated from the empty second-stage rocket motor at about 62 seconds with little or no disturbance on the three vehicles described herein. The three microswitch systems, as explained in a previous section, indicated that separation was smooth and no tilt or kick-off was encountered in the cutting of the metal and expansion of the bellows.

When the velocity stages leave the velocity-package shell propelled by the third-stage rocket motor the transmission of the telemetry data must change to a different antenna. At the instant the third stage fires, the antenna of the velocity package is disengaged and the transmission of the signal is interrupted temporarily until the whip antennas of the reentry system are extended. This temporary interruption of the signal is illustrated in figure 20, which shows a portion of a typical telemeter record from the third-stage telemeter at the time the third stage is ignited. The figure shows that it takes about 0.1 second for the reentry rocket motors to leave the package skin and about 0.15 second before the whip antennas stop shaking; thus, separation of the reentry rocket motors from the velocity package of Trailblazer IId has been accomplished.

Of the vehicles reported herein, separation of the component parts during the reentry sequence has occurred without mishap. Some separations are detected by telemetry, whereas others can only be detected by radar. The proof of separation of the small parts of Trailblazer IIb could only be detected by the velocity differential between the reentry stages as indicated by radar and optical equipment. In Trailblazer IId separation of the payload was detected by telemetry. Figure 21 shows three portions of the telemeter record from the fourth-stage telemeter. The section on the left shows the fourth-stage ignition on the longitudinal acceleration trace. The middle section shows the separation of the 8-inch spherical payload from the fourth stage detected by a separation switch designed to change the telemeter frequency when separation occurs. The section on the right shows the ignition of the fifth-stage retro-rocket motor on the longitudinal acceleration trace. The sections of the telemeter record indicate that these separations and rocket-motor firings worked as expected.

Reentry Results

Presented herein are some optical and radar data obtained during the reentry of the payloads into the atmosphere. The analysis of these data is beyond the scope of this report, but figures 22 and 23 are presented to show the type of data obtained and to indicate that the specific flight was successful from the standpoint of obtaining reentry data. Photographs taken from Coquina Beach, North Carolina, of the reentry streaks from the three vehicles presented herein are shown in figure 22. These photographs show not only the payload reentry streak but also the reentry streaks of the burned-out rocket motors and occasionally other debris released from the reentry system. In each case the photograph includes all the reentry objects that were present for each shot. Some cameras were equipped with a rotating shutter which cut off the light entering the camera for short precisely measured intervals. This gave an interrupted or chopped trace on the streak photograph from which velocity calculations could be made. The traces on the photographs presented in figure 22 are unchopped, but other photographs not shown here were time chopped so that velocity calculations of the reentry object could be made. In figure 22(b), the track of the pellet is at an angle to the track of the fifth-stage rocket motor, which, as mentioned previously, indicates that a large wobble angle was present. The velocity data for the pellet were obtained from chopped photographs. It was not possible to check this velocity with radar data since the radars cannot track an object as small as the pellet. Other payloads were tracked by radar and their photographic and radar velocity data can be compared. The variation of radar cross section

with altitude of the S-band frequency is presented in figure 23. Velocity-altitude plots are also presented to be used as a comparison with the cross-section plot. The Trailblazer IIa data of S-band frequency (fig. 23(a)) are presented at the rate of 10 points/sec. The Trailblazer IId data of S-band frequency (fig. 23(b)) are presented at the rate of 40 points/sec. The data of Trailblazer IIa are quite scattered, but the data of Trailblazer IId are well defined and show enhancement quite readily. These data are presented for academic reasons and no analysis will be presented herein.

SUMMARY OF RESULTS

The results of three flight tests of an unguided reentry physics research vehicle, consisting of four basic stages and capable of reentering a payload in a near vertical trajectory at a point about 750,000 feet from the launch pad, are as follows:

1. One vehicle reentered a 45.3-pound payload at 19,700 ft/sec.

2. One vehicle used an added stage and a high-energy accelerator to reenter a 2.2-gram steel pellet at 38,900 ft/sec. This velocity was lower than expected and is believed to be due to excessive wobble at the time of accelerator ignition.

3. One vehicle reentered a solid beryllium 17.8-pound sphere at a velocity of 18,800 ft/sec. The sphere was ejected from the expended fourth-stage rocket case, and the rocket case was then slowed down with a retro-rocket to obtain the desired separation between the reentering objects.

4. All stages landed within the expected nominal dispersion ellipses except for the expended first stage. The first-stage rocket case was aerodynamically unstable when separated from the remainder of the vehicle and impacted much closer to the launch point than originally calculated. A new dispersion ellipse for this stage has been determined.

5. Approximate wobble angles at various stages throughout the flight have been determined from available telemeter records.

6. It was possible to construct pressure curves of the third-stage rocket motor and a thrust curve of the fourth-stage rocket motor from telemetered pressures and accelerations. These data indicated that the thrust of the spinning motor is somewhat similar to that of a nonspinning motor under static tests corrected to vacuum conditions except that there was a definite tendency of the thrust from the flight test to be lower during the first part of the thrust period and higher during the latter part than the thrust from the static tests.

Langley Research Center,
National Aeronautics and Space Administration,
Langley Station, Hampton, Va., July 16, 1964.

REFERENCES

1. Hansen, C. Frederick: Approximations for the Thermodynamic and Transport Properties of High-Temperature Air. NASA TR R-50, 1959. (Supersedes NACA TN 4150.)

2. Huber, Paul W.: Hypersonic Shock-Heated Flow Parameters for Velocities to 46,000 Feet Per Second and Altitudes to 323,000 Feet. NASA TR R-163, 1963.

3. Gardner, William N., Brown, Clarence A., Jr., Henning, Allen B., Hook, W. Ray, Lundstrom, Reginald R., and Ramsey, Ira W., Jr.: Description of Vehicle System and Flight Tests of Nine Trailblazer I Reentry Physics Research Vehicles. NASA TN D-2189, 1964.

4. Brown, Clarence A., Jr., and Keating, Jean C.: Flight Test Performance and Description of a Rocket Vehicle for Producing Low-Speed Artificial Meteors. NASA TN D-2270, 1964.

5. Jewell, W. O., and Wineman, A. R.: Preliminary Analysis of a Simulated Meteor Reentry at 9.8 Kilometers Per Second. NASA TN D-2268, 1964.

6. Pitts, William C., Nielsen, Jack N., and Kaattari, George E.: Lift and Center of Pressure of Wing-Body-Tail Combinations at Subsonic, Transonic, and Supersonic Speeds. NACA Rep. 1307, 1957.

7. Carraway, Ausley B., Edwards, Frederick G., and Keating, Jean C.: Investigation of the Static Stability Characteristics of Two Stages of a Three-Stage Missile at a Mach Number of 4.00. NASA TN D-651, 1961.

8. Brown, Clarence A., Jr., and Putnam, Lawrence E.: Static Aerodynamic Characteristics of a Three-Stage Rocket Vehicle Having Various Fin Configurations at Low Subsonic Mach Numbers and Angles of Attack up to 28°. NASA TN D-1786, 1963.

9. Piland, Robert O.: Summary of the Theoretical Lift, Damping-in-Roll, and Center-of-Pressure Characteristics of Various Wing Plan Forms at Supersonic Speeds. NACA TN 1977, 1949.

10. Gillis, Clarence L., and Chapman, Rowe, Jr.: Summary of Pitch-Damping Derivatives of Complete Airplane and Missile Configurations as Measured in Flight at Transonic and Supersonic Speeds. NACA RM L52K20, 1953.

11. Martz, C. William, and Swain, Robert L.: Experimental and Analytical Study of Rolling-Velocity Amplification During the Thrusting Process for Two 10-Inch-Diameter Spherical Rocket Motors in Free Flight. NASA TM X-75, 1959.

12. Henning, Allen B., Lundstrom, Reginald R., and Keating, Jean C.: A Wind-Compensation Method and Results of Its Application to Flight Tests of Twelve Trailblazer Rocket Vehicles. NASA TN D-2053, 1964.

TABLE I.- VEHICLE PHYSICAL PROPERTIES

Time, sec	Event	Weight, lb	Center of gravity, in.	I, slug-ft^2	I_X, slug-ft^2
	Trailblazer IIa				
0	Launch	13,430	425	63,800	526
1.9	Recruit burnout	12,399	417	60,000	453
35.1	Clamp release	5,576	329	40,500	260
35.6	Skat ignition	3,092	196	8,150	41.7
43.8	Skat burnout	1,888	155	5,680	35.4
62.1	Velocity-package separation	1,082	73.4	400	13.7
328.7	Altair ignition	681	86.7	62.2	6.0
368.0	Altair burnout	225	93.9	33.2	1.33
379.2	Cygnus 15 ignition	146	109.0	1.99	.90
384.0	Cygnus 15 burnout	45.3	114.0	1.15	.40
401.0	Payload reentry	45.3	114.0	1.15	.40
	Trailblazer IIb				
0	Launch	13,488	425	64,100	528
1.9	Recruit burnout	12,457	420	60,300	455
35.8	Clamp release	5,614	337	40,800	262
36.2	Skat ignition	3,092	200	8,000	40.9
44.4	Skat burnout	1,888	159	5,530	34.5
61.9	Velocity-package separation	1,055	73.0	390	13.4
329.7	Altair ignition	681	75.9	62.0	6.0
-----	Altair burnout	225	88.9	27.6	1.32
369.6	Cygnus 15 ignition	113	107.8	.79	.58
374.4	Cygnus 15 burnout	14.3	110.0	.32	.06
377.6	Cygnus 5 ignition	4.96	121.6	.0073	.0024
378.9	Cygnus 5 burnout	1.21	123.4	.0046	.00036
381.4	High-energy accelerator ignition	.005	-----	----------	---------
	Trailblazer IId				
0	Launch	13,421	427	63,800	526
1.9	Recruit burnout	12,387	419	60,000	453
35.7	Clamp release	5,612	335	40,800	262
36.0	Skat ignition	3,093	200	8,150	41.7
44.2	Skat burnout	1,903	164	5,730	35.7
62.6	Velocity-package separation	1,104	74.0	408	14.0
320.4	Altair ignition	703	78.1	64.2	6.2
359.7	Altair burnout	233	98.3	34.4	1.38
365.4	Cygnus 15 ignition	150	111.0	2.69	.70
371.4	Cygnus 15 burnout	48.3	119.2	1.70	.19
374.1	Payload ejection	17.8	128.0	.024	.024

TABLE II.- AERODYNAMIC PARAMETERS FOR THE TRAILBLAZER II VEHICLE

(a) Complete vehicle

M	$C_{l_p}\frac{d^2}{2}S$	$C_{l_\delta}\delta$	$C_{m_q}\frac{d^2}{2}S$	$C_{m_{\dot{\alpha}}}\frac{d^2}{2}S$
0	-1,028.65	0	-15,132.04	-8,107
.7	-1,245.21	0	-17,135.00	-9,610
1.1	-1,732.47	0	-36,706.00	-23,618
1.7	-1,096.33	0	-18,962.00	-7,511
3.0	-609.07	0	-15,213.00	-2,802
4.0	-460.19	0	-14,605.00	-1,922
5.0	-365.44	0	-16,269.00	-1,573

M	C_NS for angles of attack of -						
	0°	4°	15°	20°	40°	70°	90°
0	0	9.17	39.30	37.73	77.55	86.98	109.52
.9	0	10.48	42.97	41.40	84.89	102.18	123.14
1.1	0	11.74	50.36				
2.0	0	7.70	33.01				
3.0	0	5.61	24.05				
4.0	0	4.77	20.44				
5.0	0	4.30	18.39				

M	C_AS for angles of attack of -				
	0°	4°	25°	50°	90°
0	2.15	2.04	2.57	2.10	2.10
.5	2.25	2.15	2.67	2.20	2.20
.85	3.14	3.04	3.56	3.04	3.04
.90	4.24	4.14	4.66		
.95	5.34	5.34	5.71		
1.10	5.97	6.18	6.18		
2.00	5.03	5.24	5.24		
3.00	3.77	4.03			
4.00	3.20	3.51			
5.00	2.72	3.09			

M	x_{cp}, ft, for angles of attack of -				
	0°	4°	13.5°	20°	90°
0	40.01	40.32	40.01	37.17	35.00
.9	40.50	40.50	40.01	37.17	35.00
1.1	41.17	41.17	41.17		
2.0	39.00	38.82	38.82		
3.0	37.51	37.25			
4.0	36.65	36.08			
5.0	36.08	35.15			

(b) Second stage and velocity package

M	$C_{l_p}\frac{d^2}{2}S$	$C_{l_\delta}Sd$ (a)	$C_{m_q}\frac{d^2}{2}S$	$C_{m_{\dot{\alpha}}}\frac{d^2}{2}S$	$C_{N_\alpha}S$	C_AS	x_{cp}, ft
3	-56	0.556	-2,420	0	23.8	1.72	21.00
5	-38	.324	-1,620	0	17.5	1.45	18.87
8	-24	.206	-1,355	0	14.2	1.26	17.17

[a]All four fins were deflected 1.50° for Trailblazers IIa and IIb and 1.75° for Trailblazer IId.

TABLE III.- ALTITUDE, HORIZONTAL RANGE, VELOCITY, AND FLIGHT-PATH ANGLE FOR VARIOUS EVENT TIMES

(a) Trailblazer IIa

Event	Nominal				
	Time, sec	Altitude, ft	Horizontal range, ft	Velocity, ft/sec	γ, deg
Castor ignition	0	26	0	0	80.0
Recruit ignition	.05	26	0	1	80.0
Clamp release	35.5	79,502	26,601	4,429	69.2
Skat ignition	35.8	80,744	27,073	4,432	69.2
Skat burnout	44.0	130,092	46,253	7,764	68.3
Velocity-package separation	62.0	254,671	97,122	7,220	66.8
Apogee	286.0	988,518	698,211	2,747	0
Altair ignition	330.0	959,972	813,743	3,038	-25.1
Cygnus 15 ignition	380.0	656,372	868,998	10,761	-92.6
Payload max. velocity	404.5	213,287	787,447	19,625	-100.8
Altair max. velocity	420.0	201,998	849,253	11,918	-92.4
Skat impact	547.0	0	1,395,000	1,000	-70.0

Event	Actual					
	Time, sec	Altitude, ft	Horizontal range, ft	Velocity, ft/sec	γ, deg	γ_d, deg
Castor ignition	0	26	0	0	75.3	0
Recruit ignition	.16	26	0	------	75.3	0
Clamp release	35.1	68,150	25,170	4,076	68.2	0
Skat ignition	35.6	70,040	25,920	4,070	68.1	0
Skat burnout	43.8	115,222	44,103	7,424	67.6	0
Velocity-package separation	62.1	235,000	94,730	6,876	65.9	0
Apogee	274.0	894,100	651,600	2,620	0	0
Altair ignition	328.7	849,400	793,900	3,070	-31.5	0
Cygnus 15 ignition	379.2	511,800	853,000	10,350	-88.7	-8.0
Payload max. velocity	401.0	132,000	822,000	19,780	-96.0	-11.2

TABLE III.- ALTITUDE, HORIZONTAL RANGE, VELOCITY, AND FLIGHT-PATH ANGLE FOR VARIOUS EVENT TIMES - Continued

(b) Trailblazer IIb

Event	Nominal				
	Time, sec	Altitude, ft	Horizontal range, ft	Velocity, ft/sec	γ, deg
Castor ignition	0	26	0	0	80.0
Recruit ignition	.05	26	0	1	80.0
Clamp release	35.5	79,502	26,601	4,429	69.2
Skat ignition	35.8	80,744	27,073	4,432	69.2
Skat burnout	44.0	130,092	46,253	7,764	68.3
Velocity-package separation	62.0	254,671	97,122	7,220	66.8
Apogee	286.0	988,518	698,211	2,747	0
Altair ignition	330.0	959,972	813,743	3,038	-25.1
Spin-rockets firing	368.0	742,901	858,541	10,351	-92.6
Cygnus 15 ignition	370.4	717,998	857,401	10,423	-92.6
Cygnus 5 ignition	377.3	588,704	831,031	25,882	-104.2
High-energy accelerator ignition	382.0	436,040	787,113	36,008	-106.4
Pellet max. velocity	384.8	309,645	749,996	47,075	-106.3
Cygnus 5 max. velocity	386.0	297,618	746,499	36,106	-106.3
Cygnus 15 max. velocity	389.5	280,358	753,445	26,226	-104.2
Altair max. velocity	417.0	199,737	835,314	11,788	-92.3
Skat impact	547.0	0	1,395,000	1,000	-70.0

Event	Actual					
	Time, sec	Altitude, ft	Horizontal range, ft	Velocity, ft/sec	γ, deg	γ_d, deg
Castor ignition	0	26	0	0	78.0	0
Recruit ignition	.14	26	0	------	78.0	0
Clamp release	35.8	78,413	23,822	4,189	71.4	0
Skat ignition	36.2	79,997	24,351	4,193	71.4	0
Skat burnout	44.4	128,280	40,860	7,686	70.5	0
Velocity-package separation	61.9	250,970	84,915	7,159	69.2	0
Apogee	288.0	1,000,420	619,300	2,400	0	0
Altair ignition	329.7	975,860	716,380	2,800	-26.1	0
Spin-rockets firing	367.7	786,434	773,400	10,354	-89.0	-8.8
Cygnus 15 ignition	369.6	767,630	774,000	10,686	-89.0	-8.8
Cygnus 5 ignition	377.6	618,030	758,220	25,428	-99.4	-8.5
High-energy accelerator ignition	381.4	522,440	744,820	34,200	-98.3	-7.6
Pellet top of visible trail	389.5	243,000	649,000	38,900	-----	----

TABLE III.- ALTITUDE, HORIZONTAL RANGE, VELOCITY, AND FLIGHT-PATH ANGLE FOR VARIOUS EVENT TIMES - Concluded

(c) Trailblazer IId

Event	Nominal				
	Time, sec	Altitude, ft	Horizontal range, ft	Velocity, ft/sec	γ, deg
Castor ignition	0	26	0	0	80.0
Recruit ignition	.05	26	0	1	80.0
Clamp release	35.5	79,502	26,601	4,429	69.2
Skat ignition	35.8	80,744	27,073	4,432	69.2
Skat burnout	44.0	130,092	46,253	7,764	68.3
Velocity-package separation	62.0	254,671	97,122	7,220	66.8
Apogee	286.0	988,518	698,518	2,747	0
Altair ignition	325.0	959,972	813,743	3,038	-25.1
Cygnus 15 ignition	370.0	728,776	860,013	10,037	-91.9
Payload separation	377.2	564,391	833,642	19,394	-99.5
Cygnus 5 ignition	382.2	466,473	817,752	19,540	-99.4
Payload max. velocity	394.9	220,855	777,740	19,910	-99.4
Cygnus 15 - 5 max. velocity	394.2	247,382	784,579	18,702	-98.7
Skat impact	547.0	0	1,395,000	1,000	-70.0

Event	Actual					
	Time, sec	Altitude, ft	Horizontal range, ft	Velocity, ft/sec	γ, deg	γ_d, deg
Castor ignition	0	26	0	0	75.0	0
Recruit ignition	.21	26	0	------	75.0	0
Clamp release	35.7	78,000	30,400	4,220	69.8	0
Skat ignition	36.0	79,000	30,500	4,220	69.8	0
Skat burnout	44.2	125,000	48,300	7,500	68.5	0
Velocity-package separation	62.6	247,520	92,469	6,984	67.3	0
Apogee	280.0	939,663	639,963	2,596	0	0
Altair ignition	320.4	915,900	739,900	2,860	-24.8	0
Cygnus 15 ignition	365.4	669,000	781,700	9,860	-95.0	-8.9
Payload separation	374.1	543,400	759,800	18,280	-102.0	-8.9
Cygnus 5 ignition	379.0	447,240	738,145	18,400	-102.0	-8.9
Payload max. velocity	388.0	289,000	707,000	18,800	-102.0	-8.9

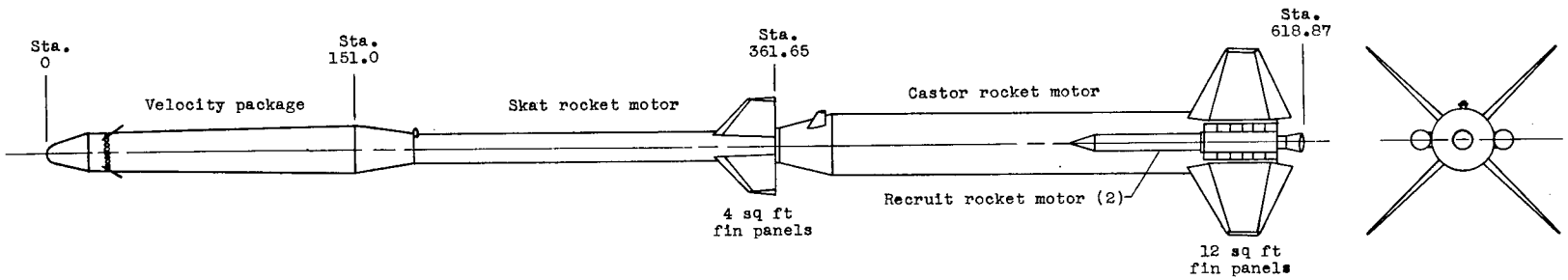

(a) First stage, second stage, and velocity package.

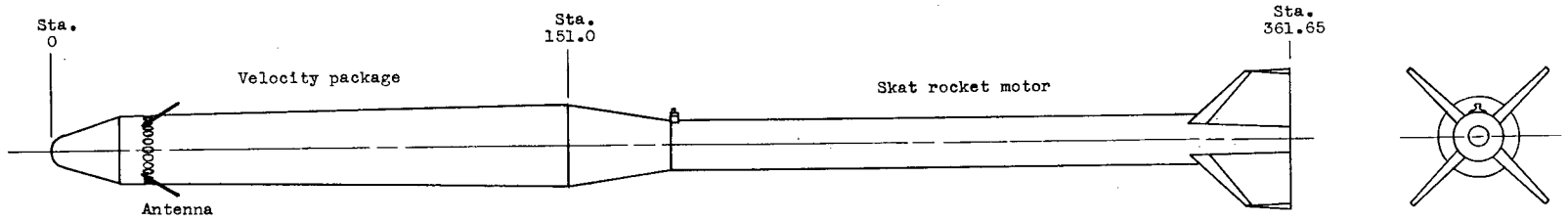

(b) Second stage and velocity package.

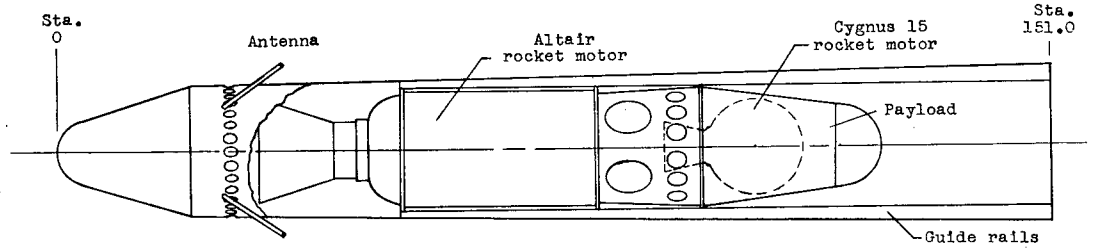

(c) Velocity package.

Figure 1.- Sketches of the Trailblazer II reentry research vehicle. All station locations are in inches.

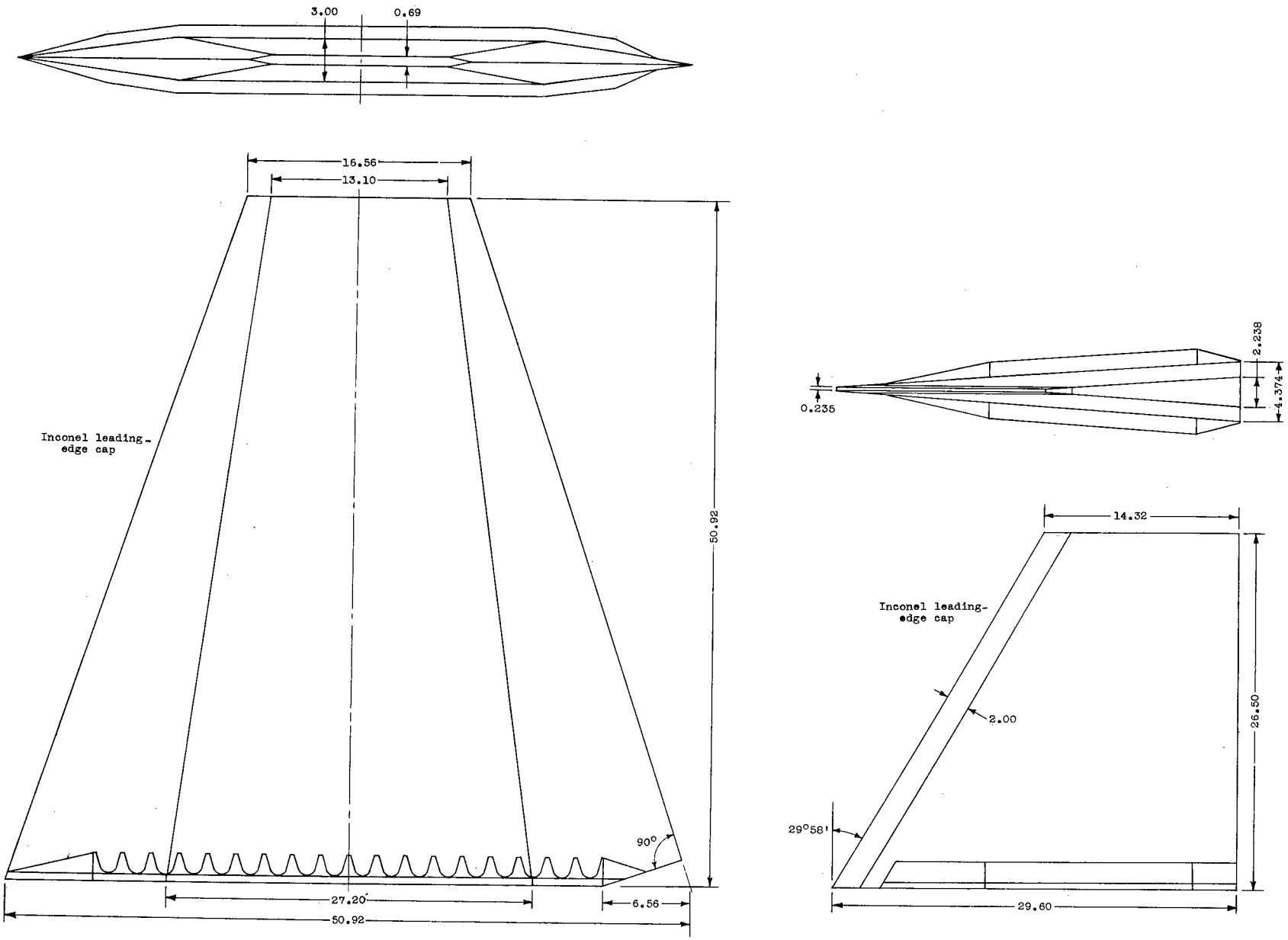

Figure 2.- Sketch of the first- and second-stage fins. All dimensions are in inches.

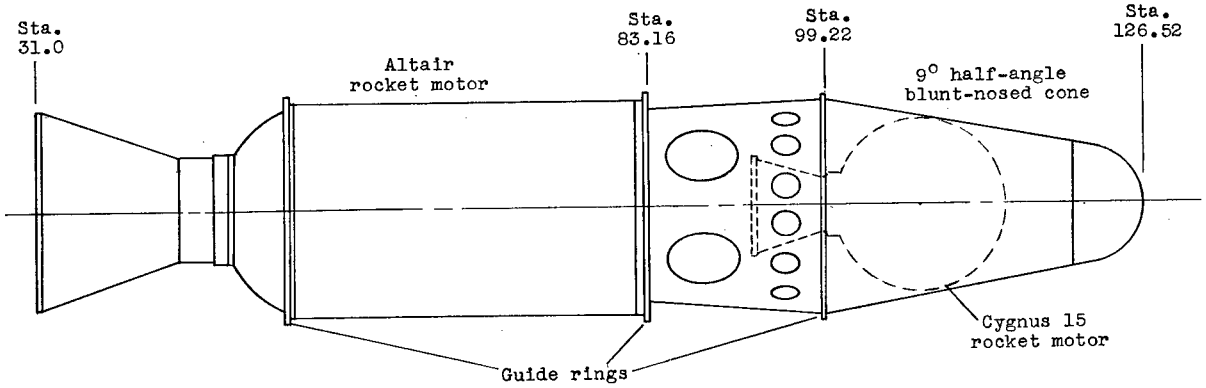

(a) Trailblazer IIa.

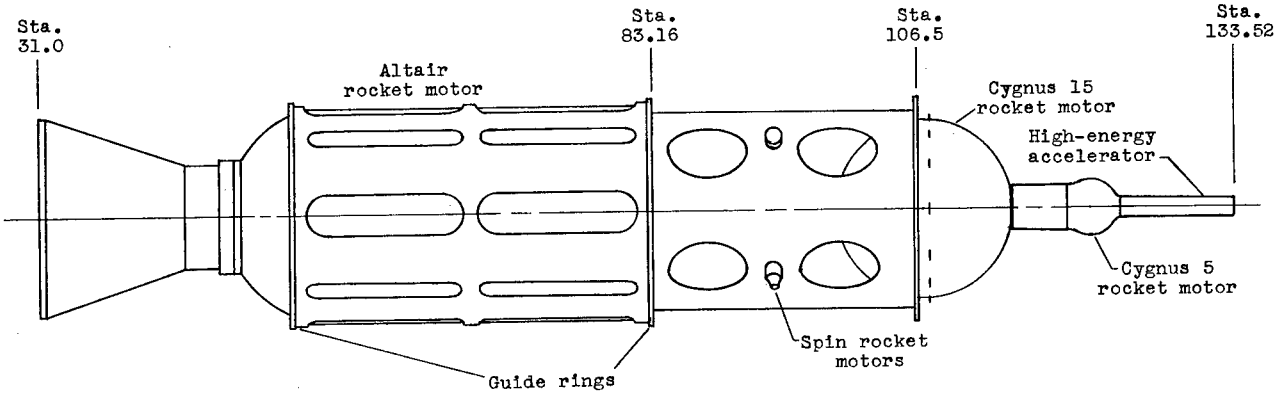

(b) Trailblazer IIb.

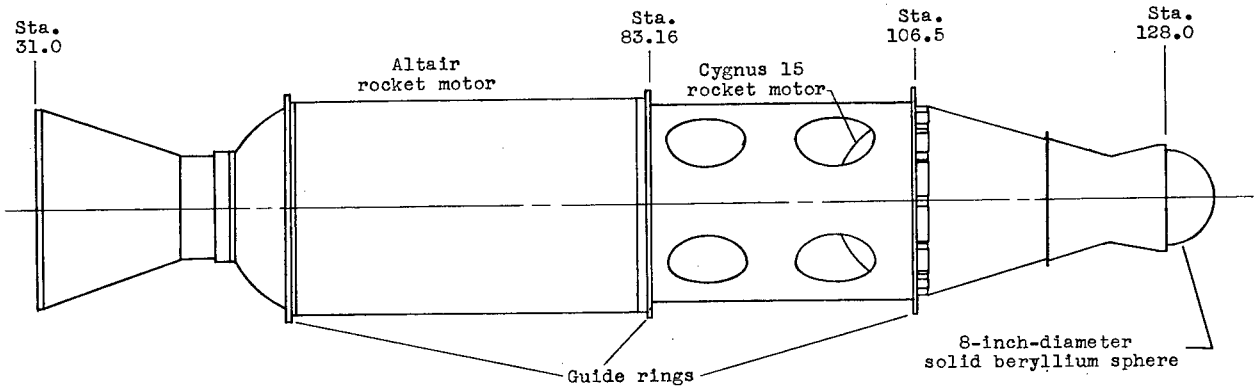

(c) Trailblazer IId.

Figure 3.- Sketches of the third-stage and payload combinations. All station locations are in inches.

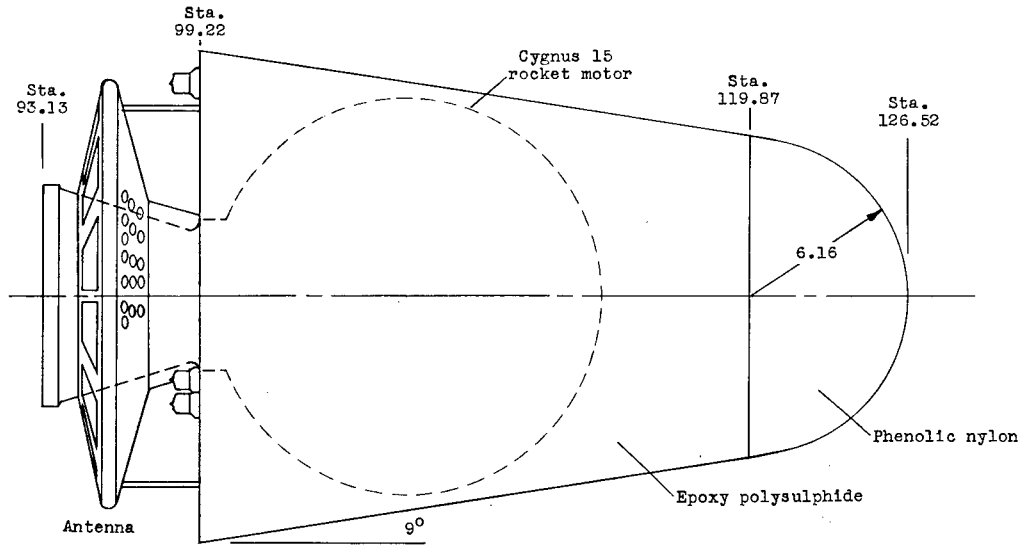

(a) Trailblazer IIa. A 9° half-angle blunt-nosed cone as the reentry object.

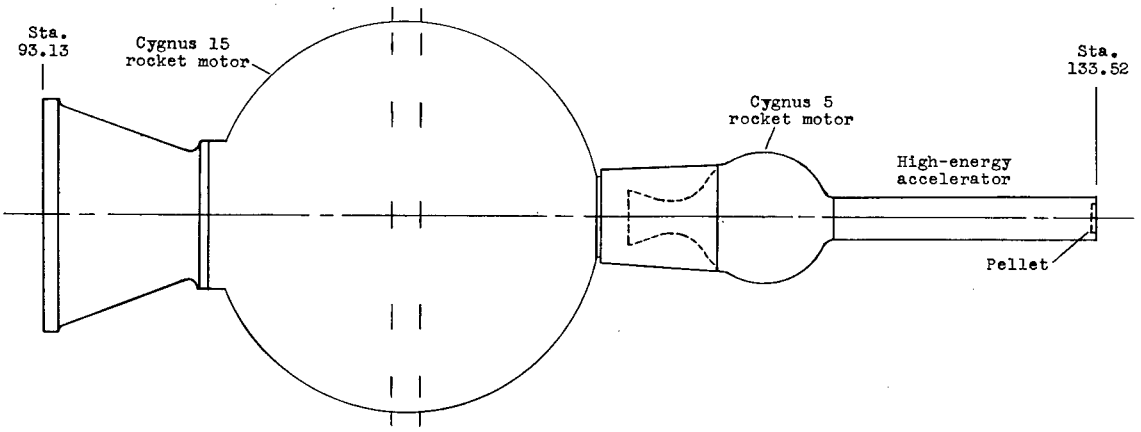

(b) Trailblazer IIb. A 5.8-gram stainless-steel pellet, the primary reentry object, propelled by Cygnus 15, Cygnus 5, and a shaped-charge accelerator.

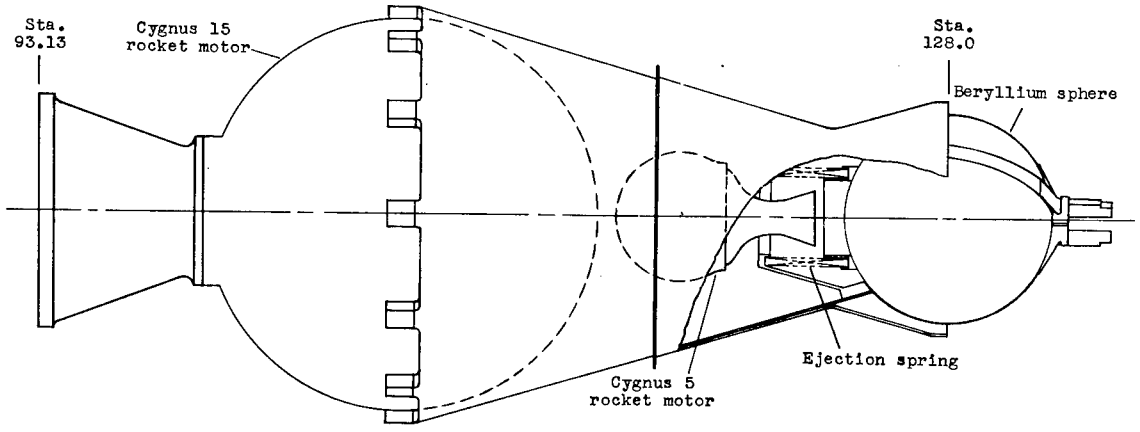

(c) Trailblazer IId. An 8-inch-diameter solid beryllium sphere, the primary reentry object, propelled by Cygnus 15 and ejected by a spring.

Figure 4.- Sketches of the payloads. All station locations are in inches.

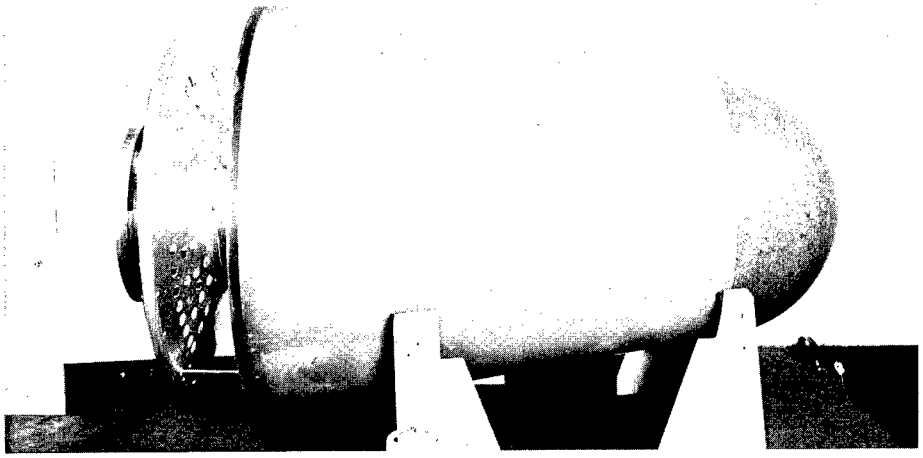

(a) Trailblazer IIa. L-61-7903

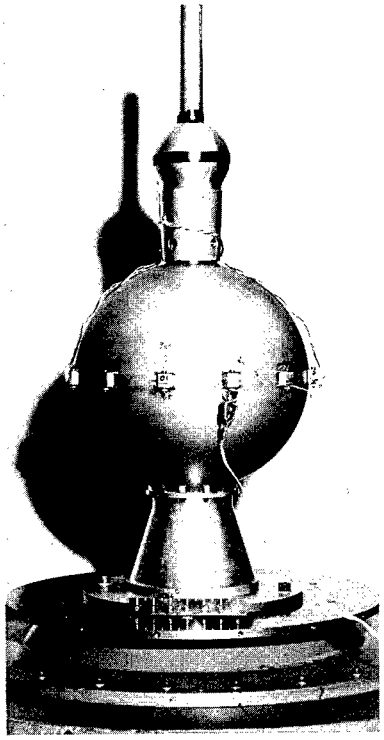

L-62-3614
(b) Trailblazer IIb.

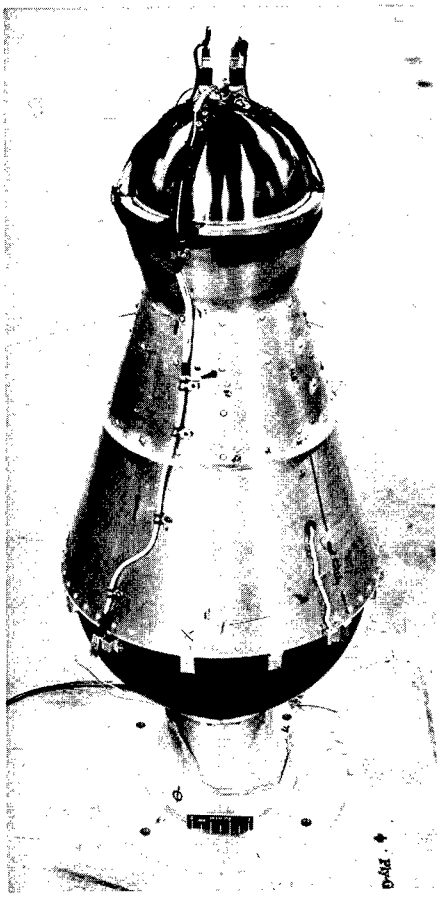

L-63-1741
(c) Trailblazer IId.

Figure 5.- Photographs of the reentry configurations.

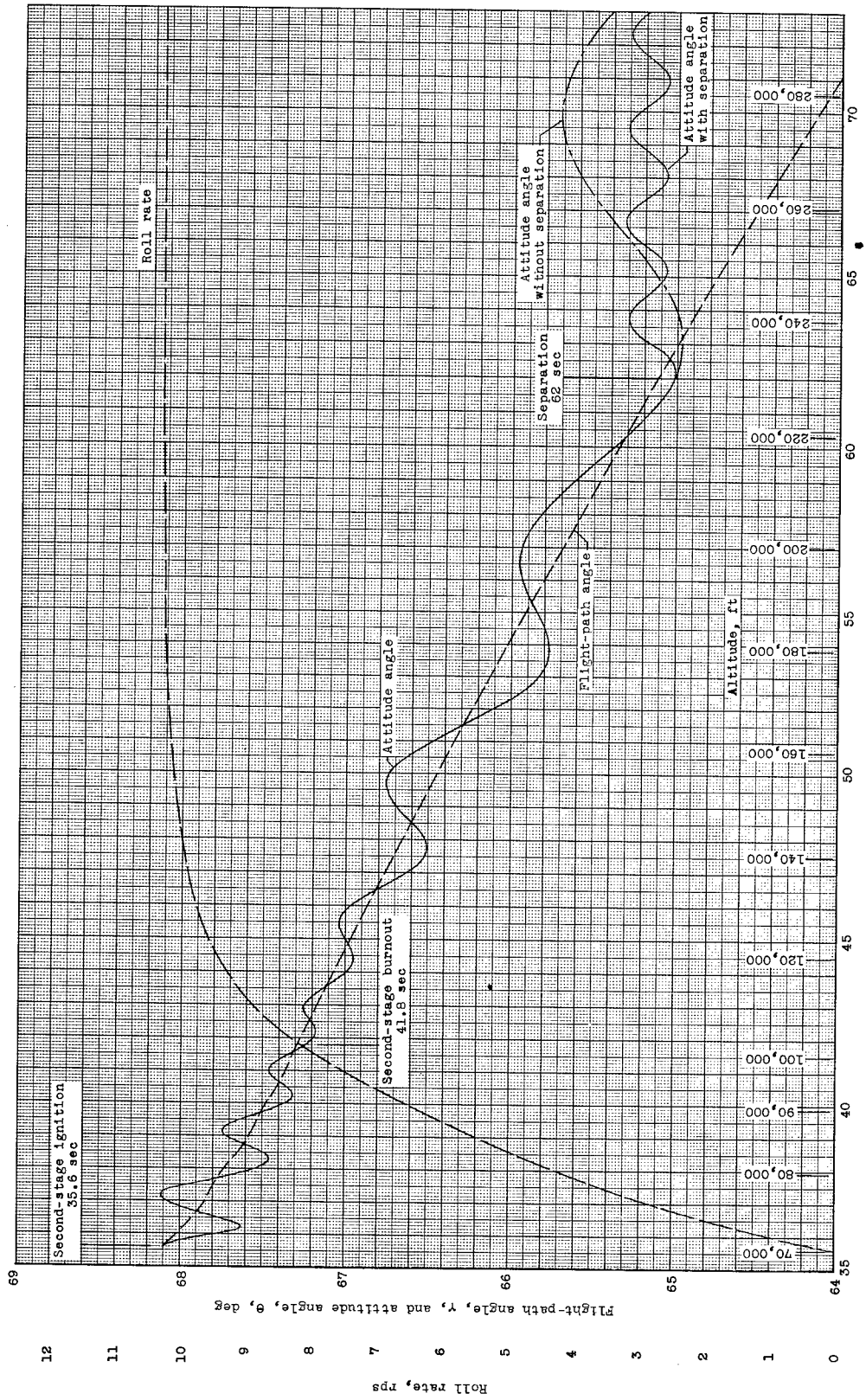

Figure 6.- Calculated time history of roll rate and vehicle attitude showing transition from aerodynamic to spin stabilization assuming a 0.05° thrust misalinement.

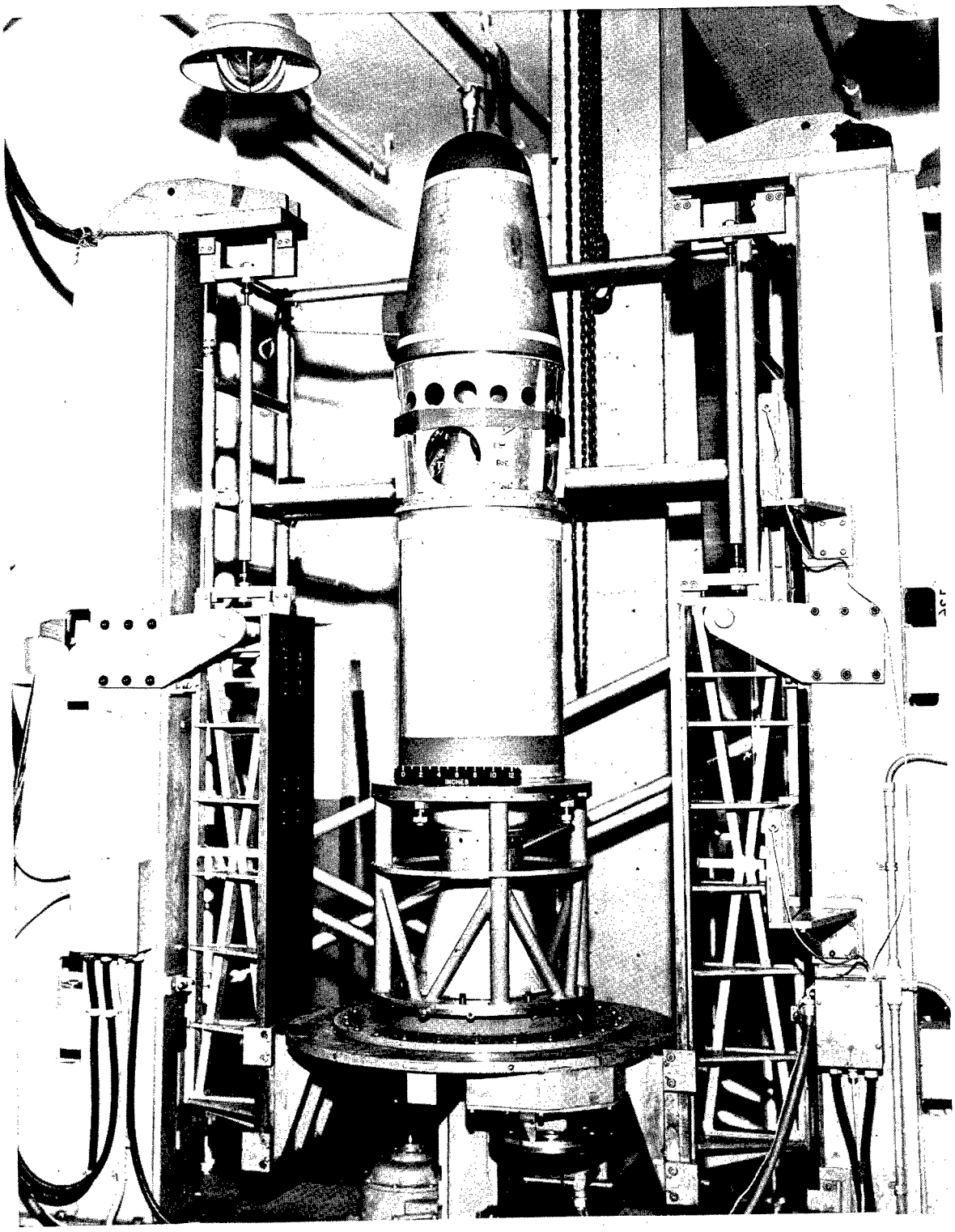

L-61-300

Figure 7.- Photograph of Trailblazer IIa reentry configuration mounted in the vertical spin balance machine.

L-61-8229

Figure 8.- Photograph of the Skat rocket motor and velocity package mounted in the horizontal spin balance machine.

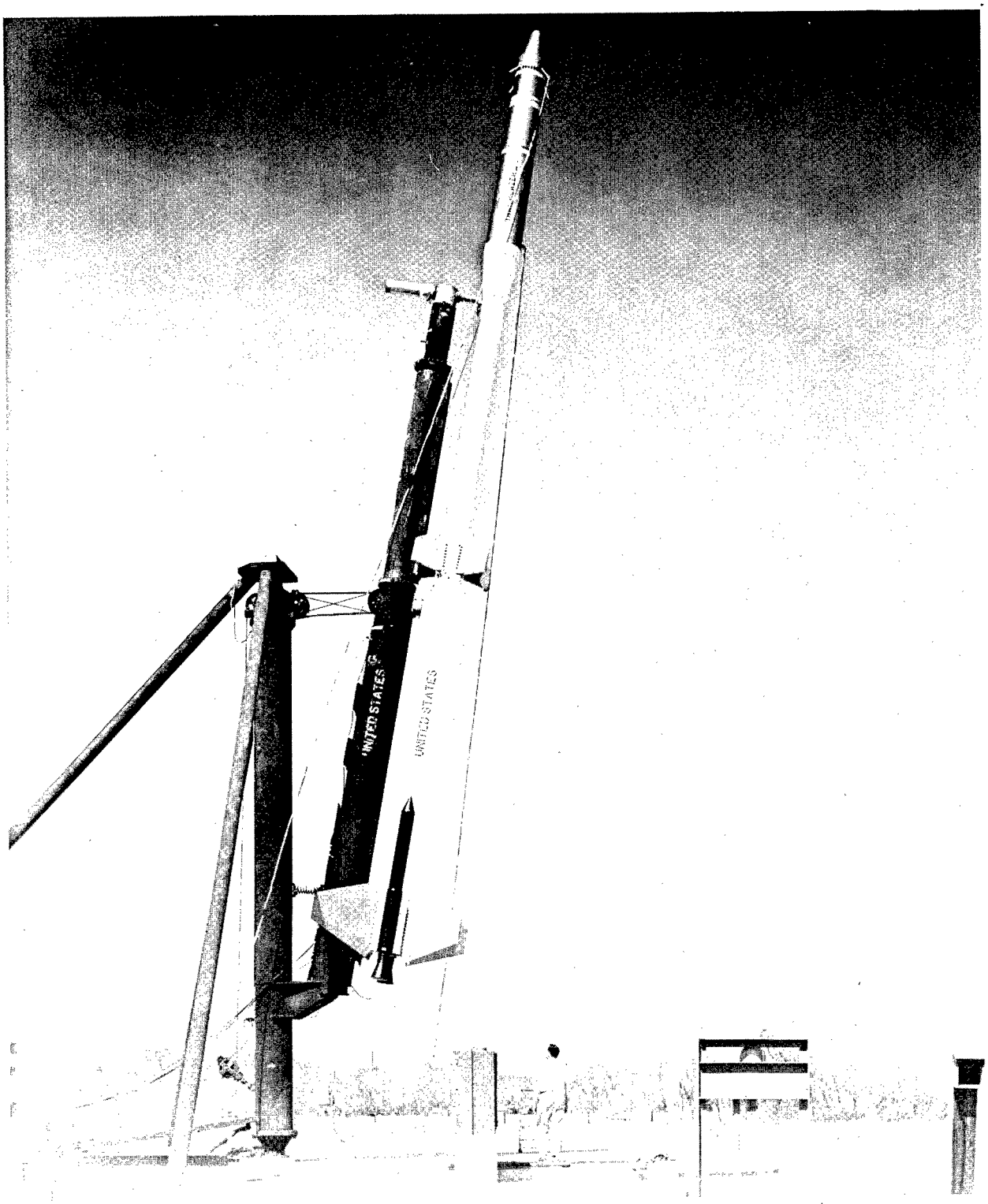

L-62-4433

Figure 9.- Photograph of the Trailblazer II reentry research vehicle on the launcher.

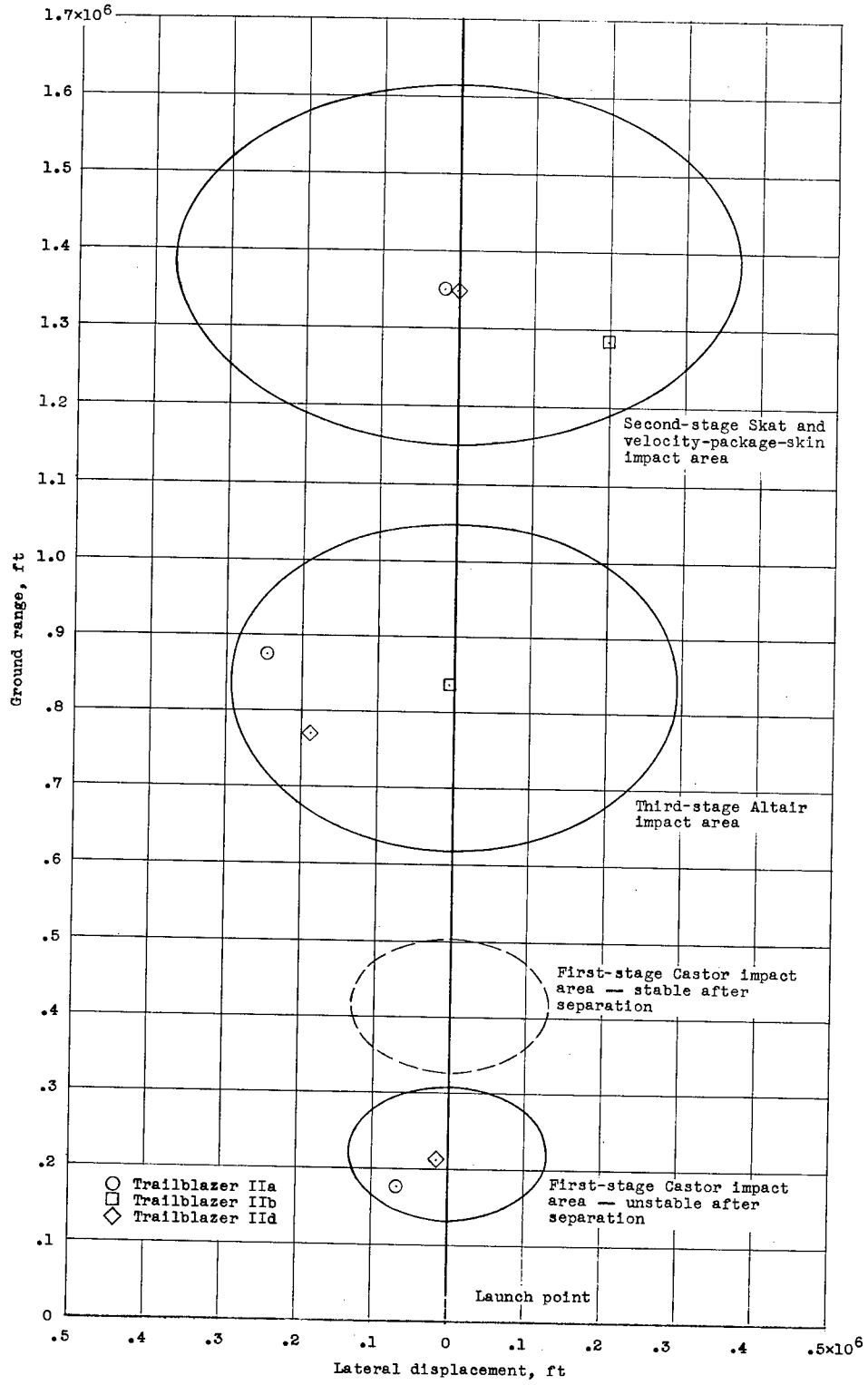

Figure 10.- Predicted impact areas for the Castor, Altair, and Skat rocket motors and the velocity-package skin, including actual impact from three Trailblazer II flight tests.

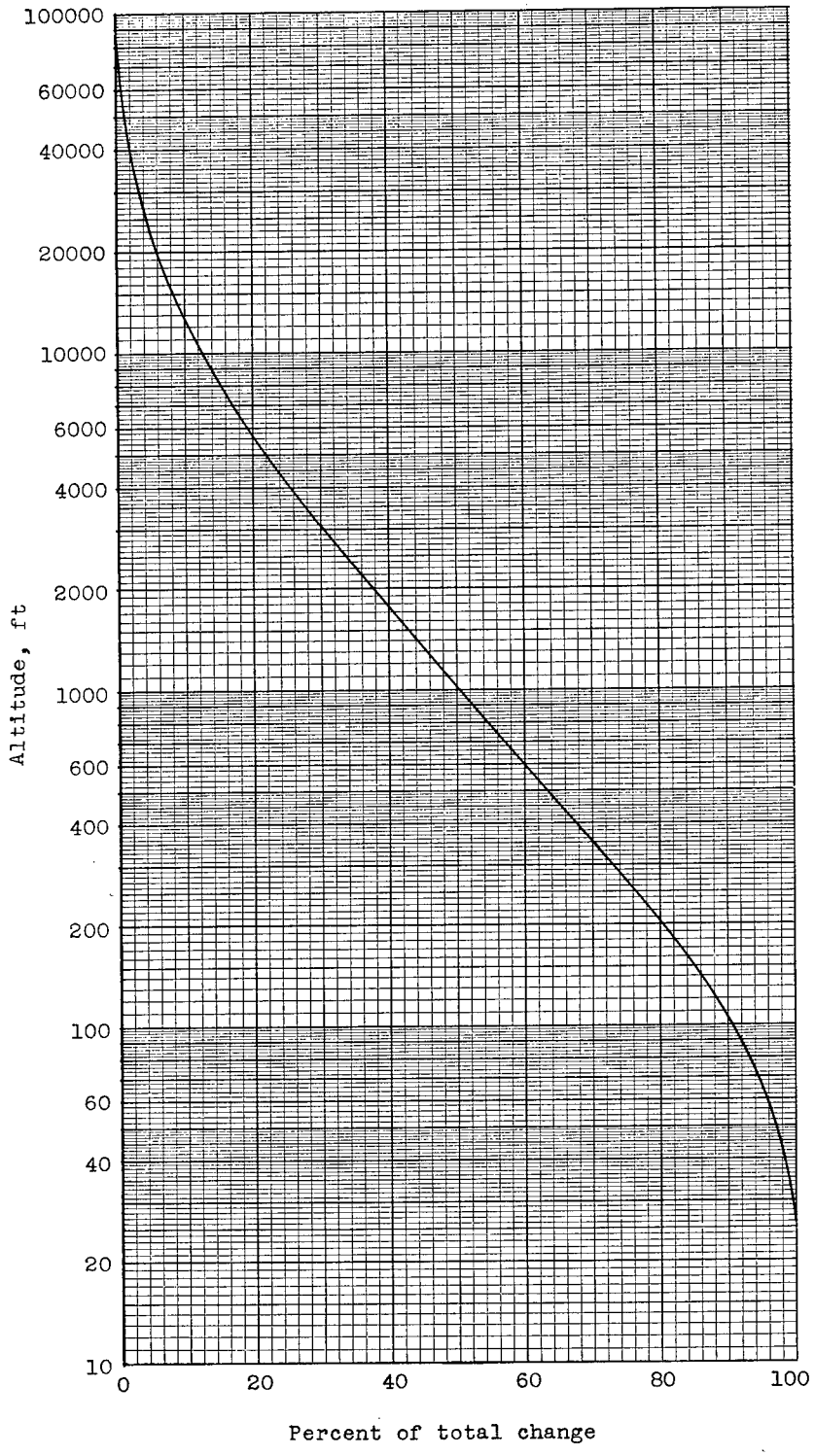

Figure 11.- Variation of altitude with percent of total change in flight-path angle from a constant wind for the Trailblazer II vehicle.

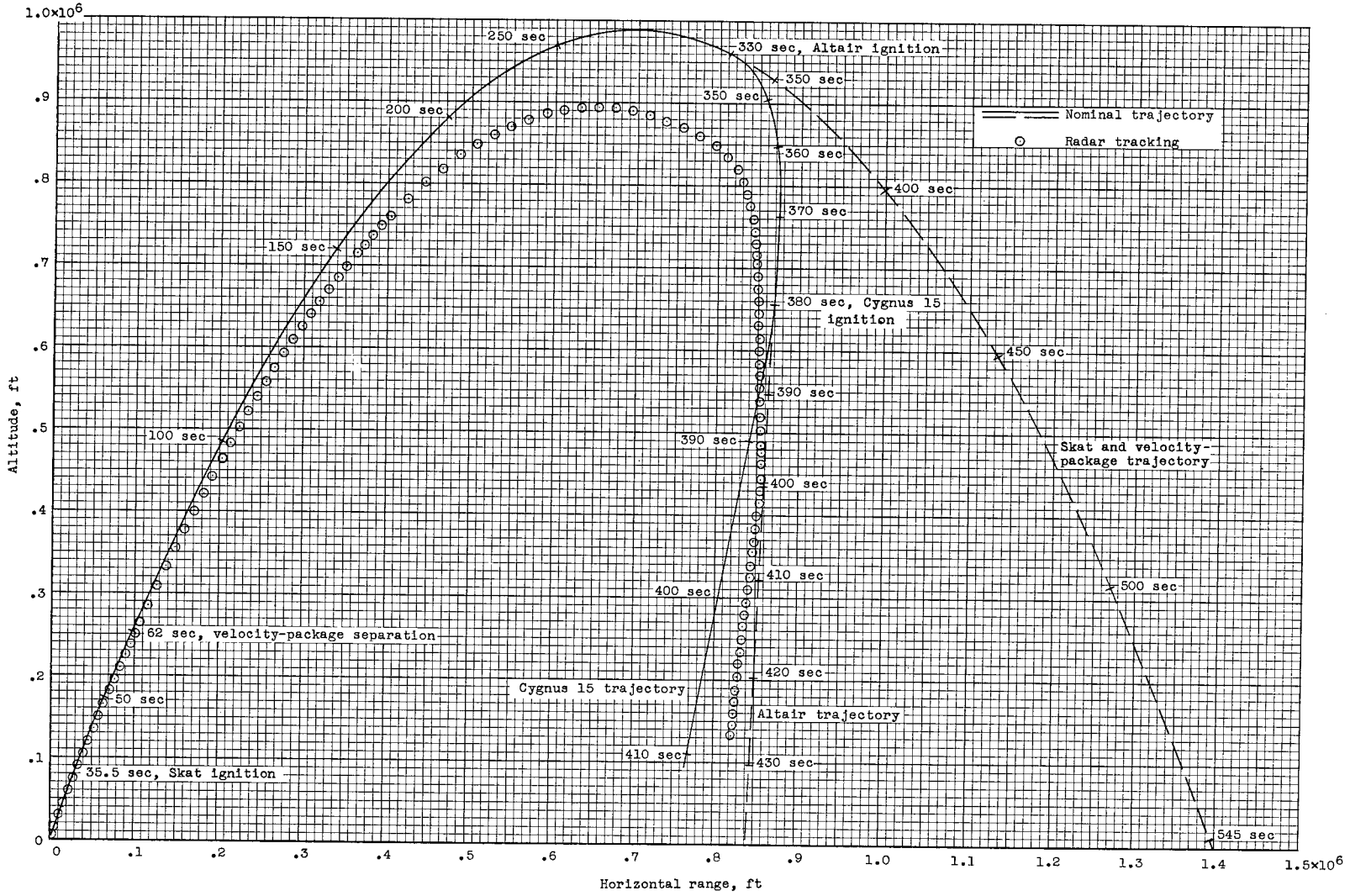

(a) Trailblazer IIa.

Figure 12.- Comparison of the variation of altitude with horizontal range between the predicted flight path and radar tracking of three Trailblazer II vehicles.

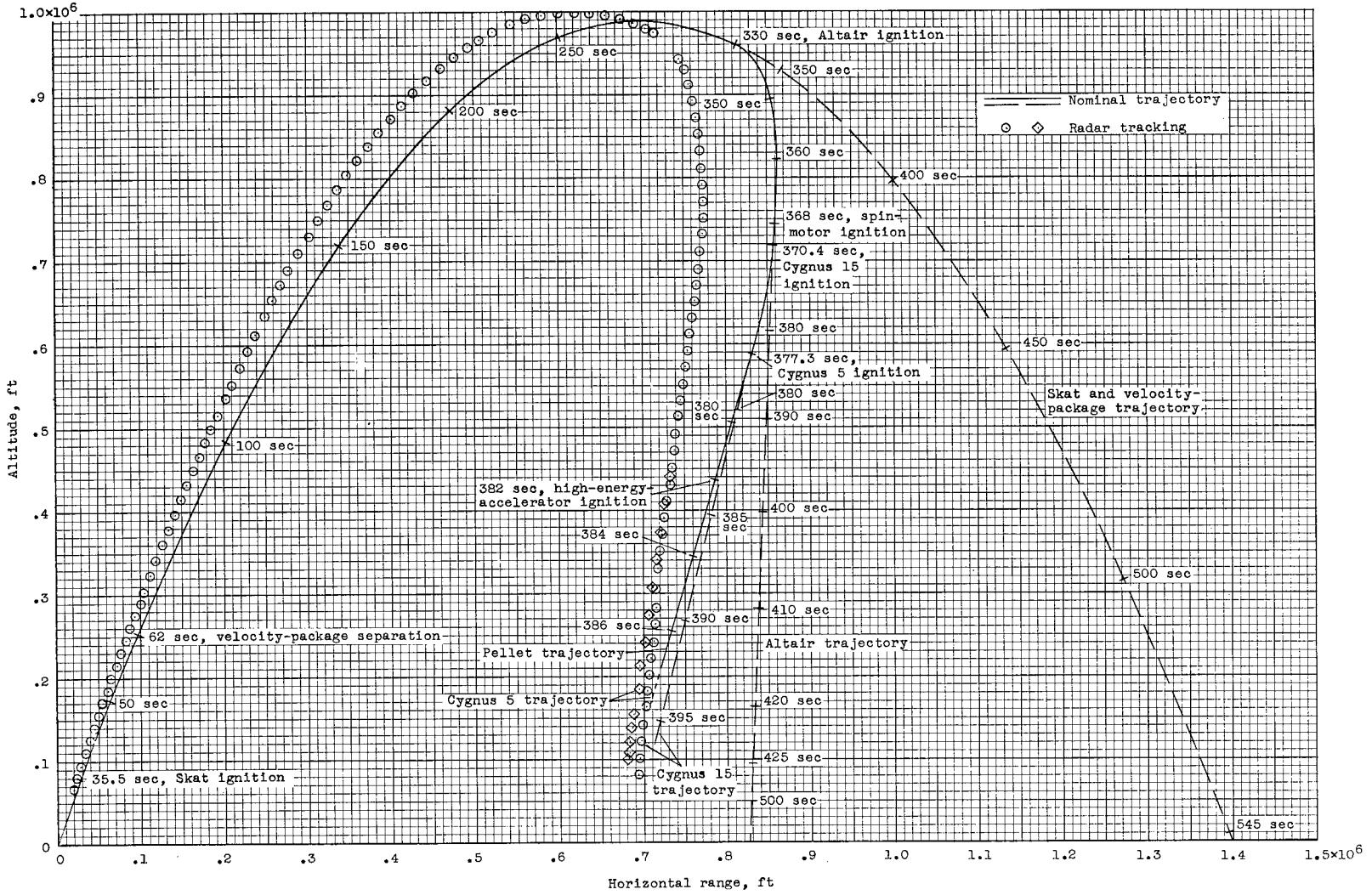

(b) Trailblazer IIb.

Figure 12.- Continued.

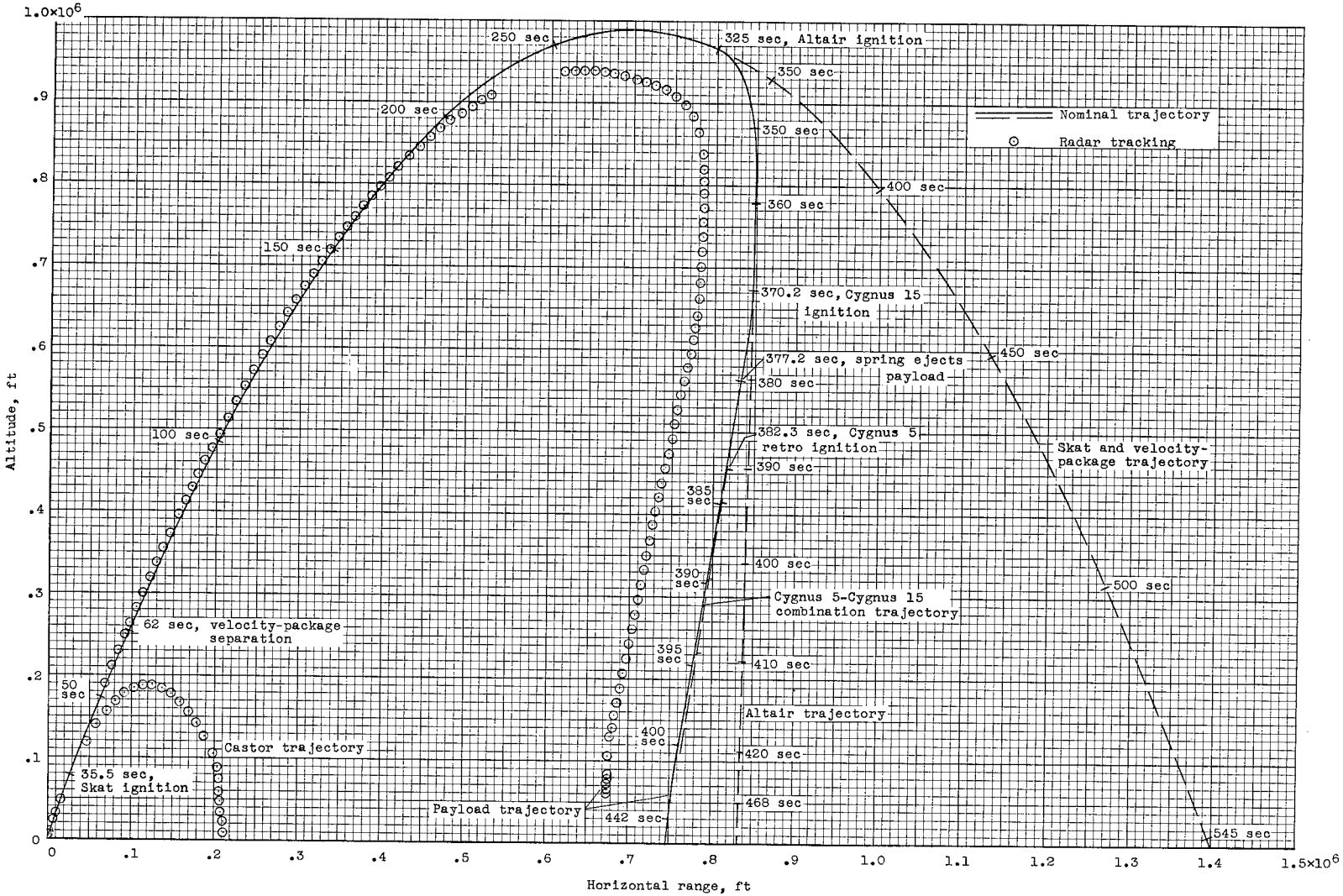

(c) Trailblazer IId.

Figure 12.- Concluded.

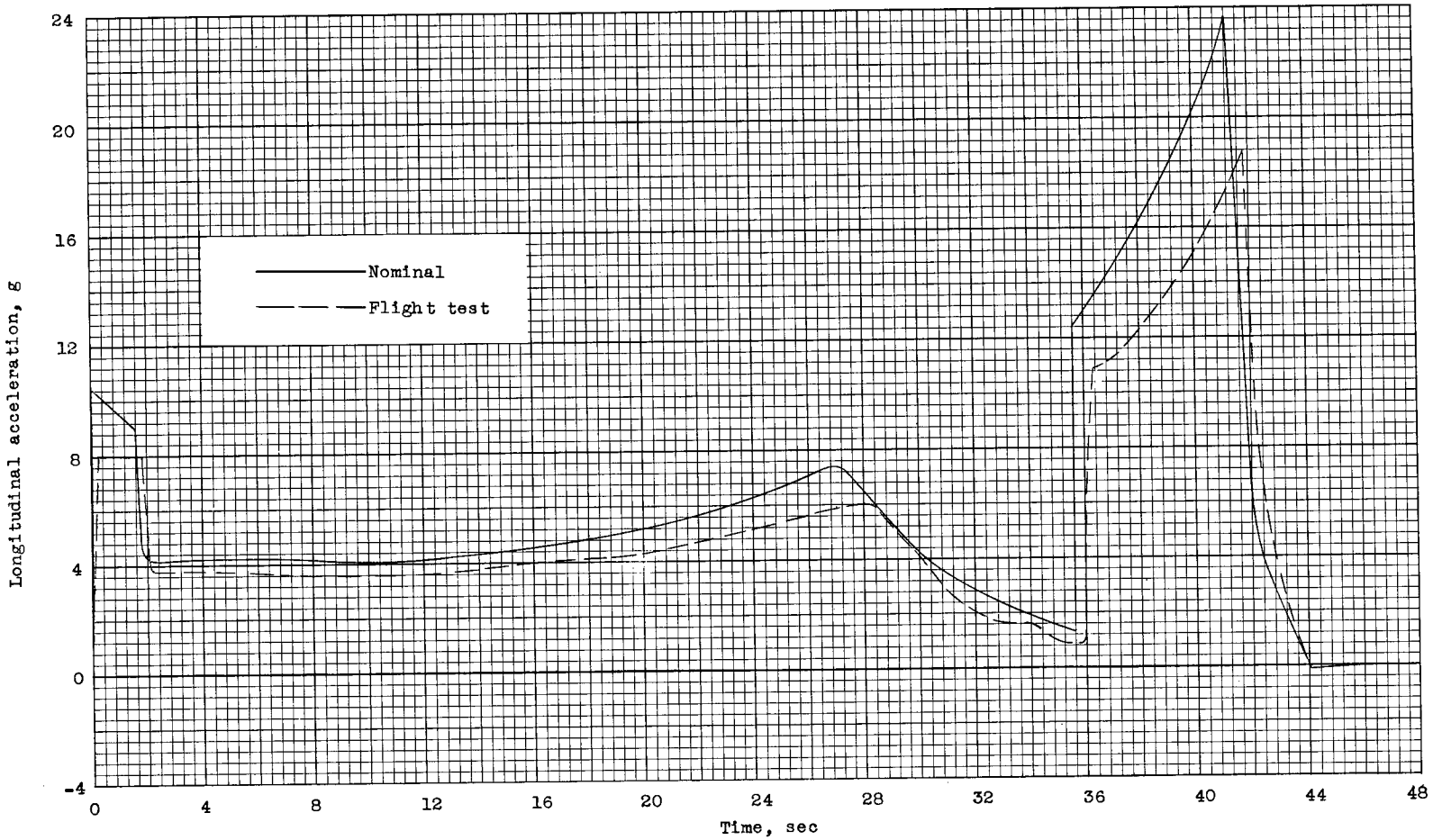

(a) Axial acceleration of first and second stages.

Figure 13.- Variation of axial acceleration with time for a typical Trailblazer II flight.

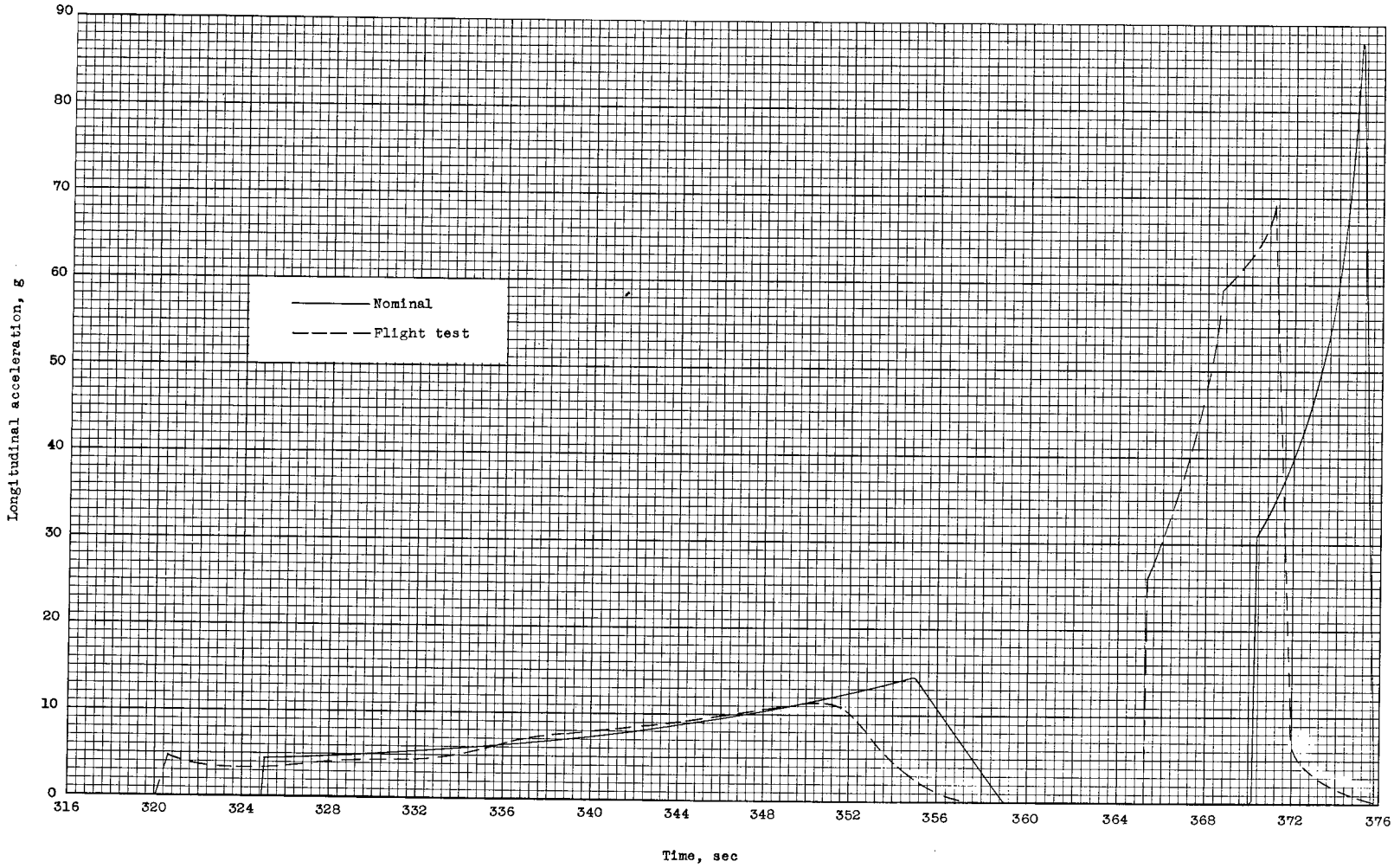

(b) Axial acceleration of reentry stages.

Figure 13.- Concluded.

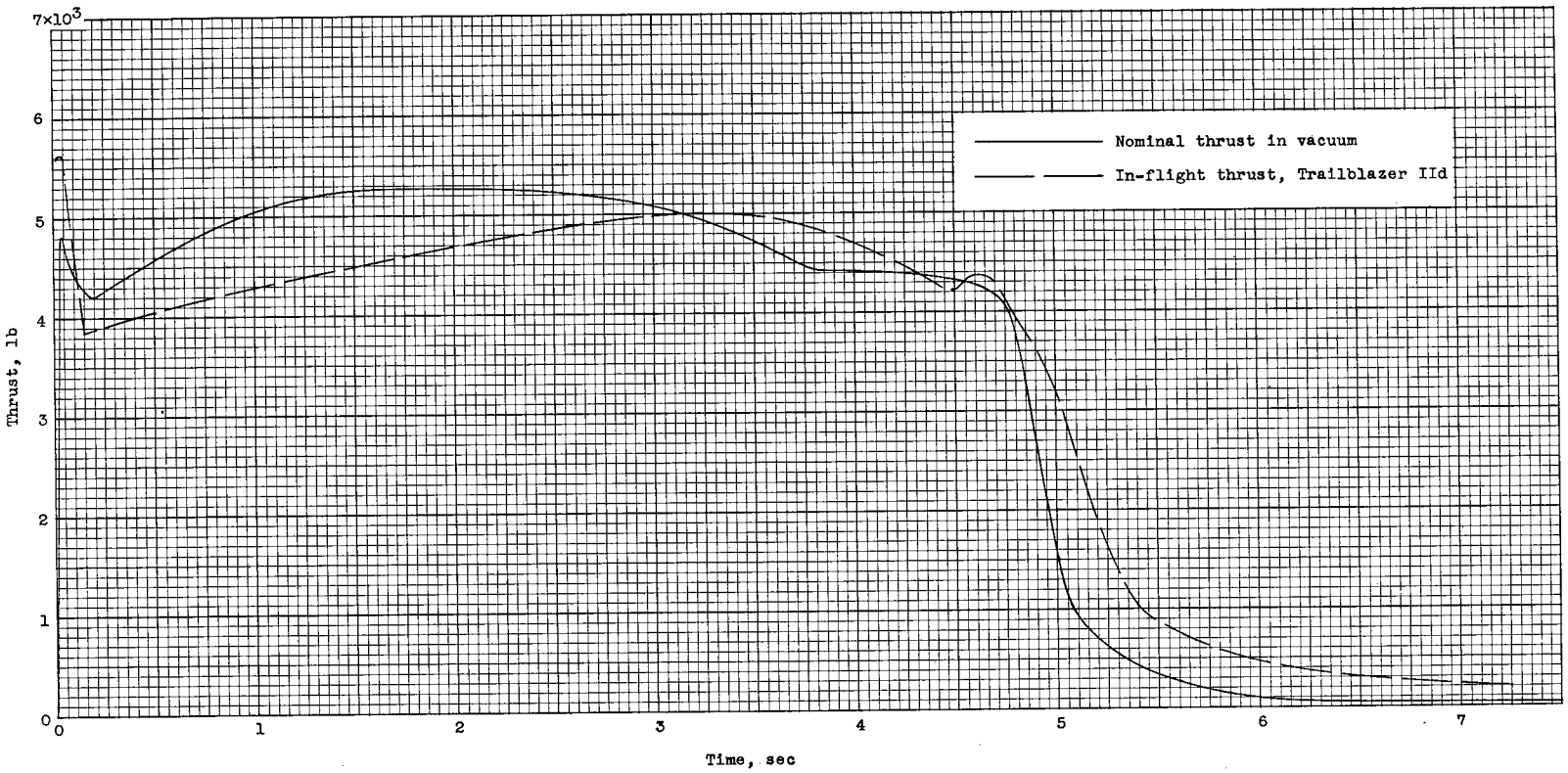

Figure 14.- In-flight thrust of the Cygnus 15 rocket motor of Trailblazer IId compared with nominal values in vacuum.

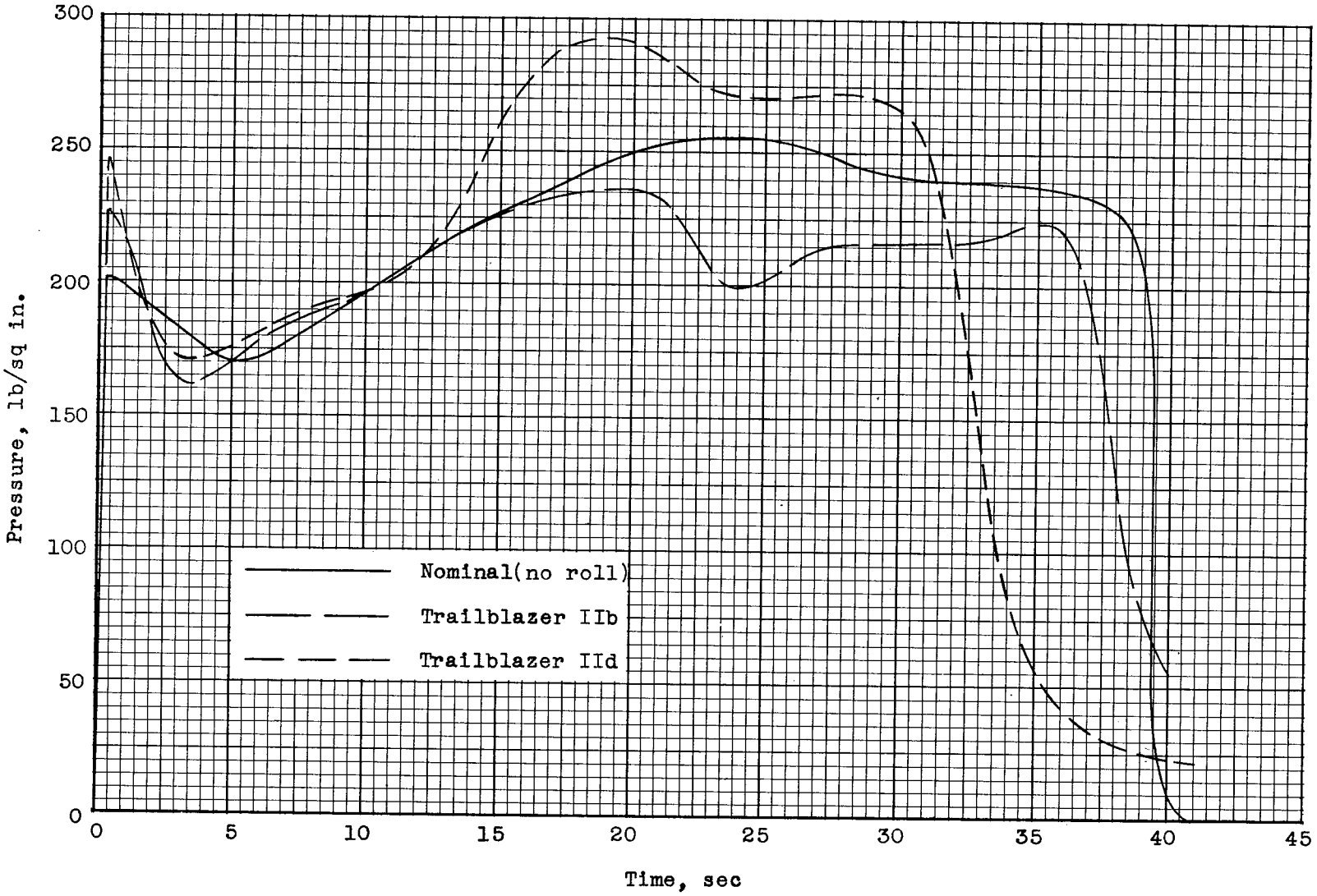

Figure 15.- In-flight chamber pressure of the Altair rocket motor of Trailblazers IIb and IId compared with nominal values.

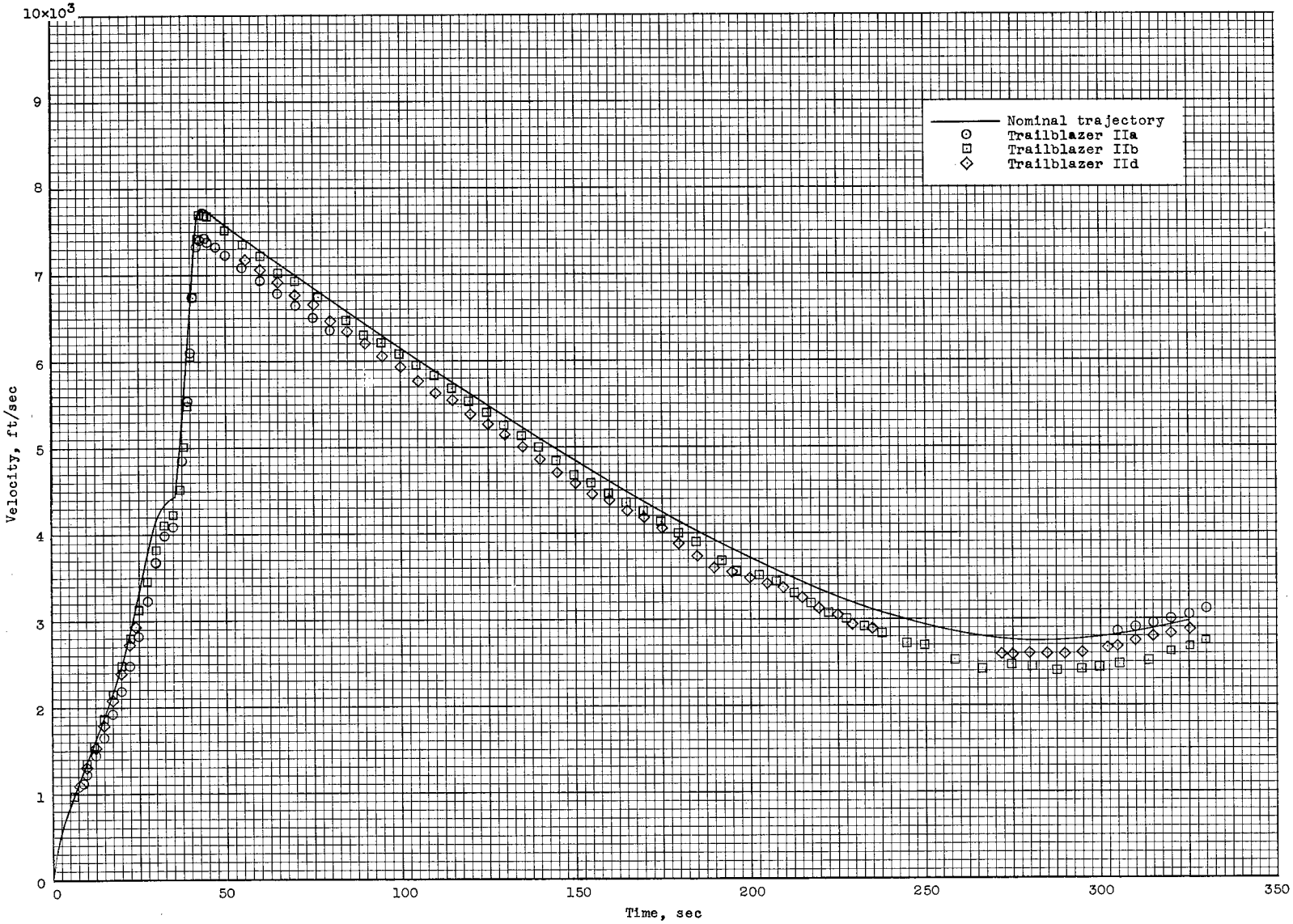

Figure 16.- Comparison of estimated velocity as a function of time from launch to apogee with values obtained by radar tracking for flights of three Trailblazer II vehicles.

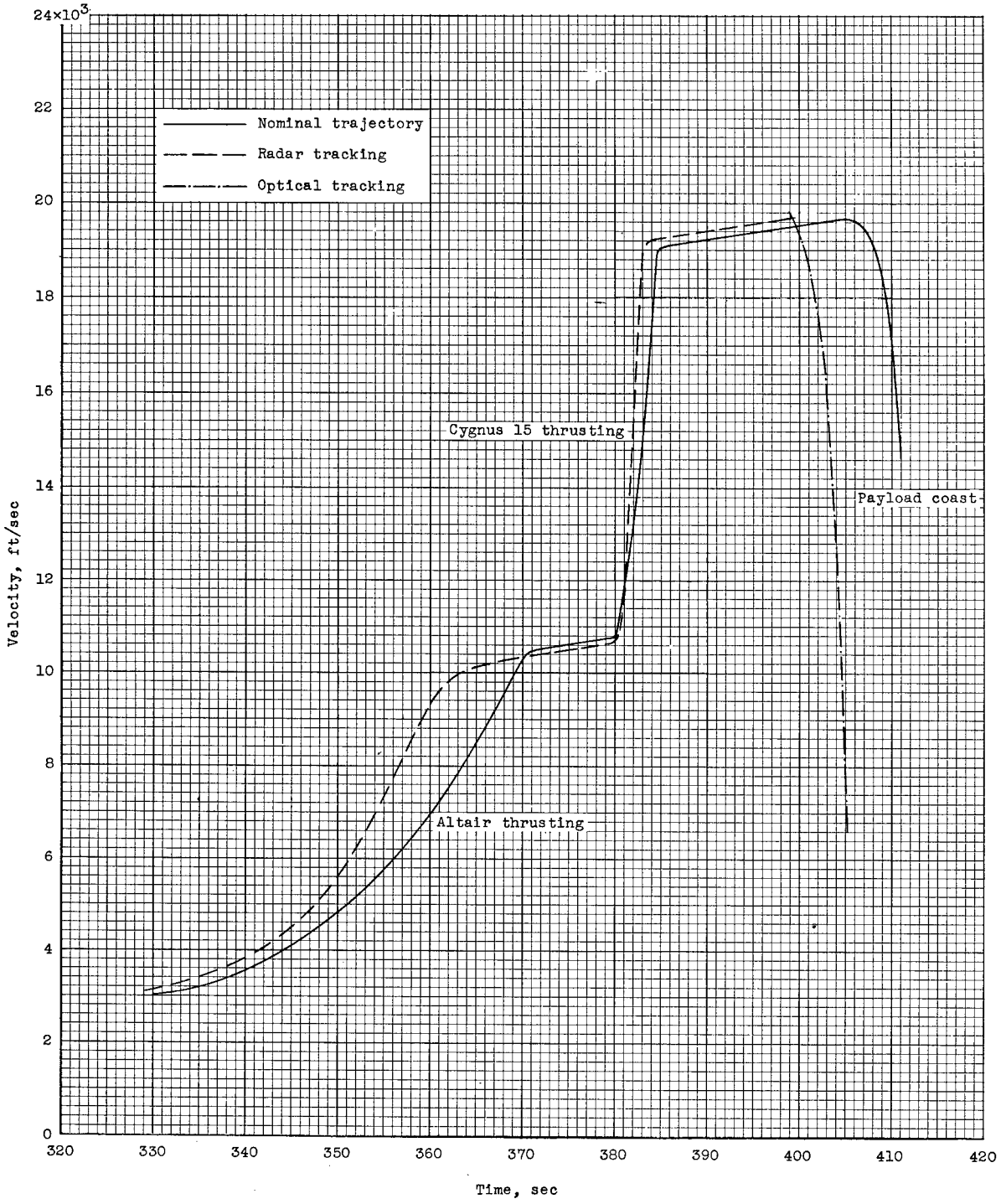

(a) Trailblazer IIa.

Figure 17.- Comparison of estimated velocity as a function of time for the reentry portion of the flight of three Trailblazer II vehicles with values obtained by radar tracking.

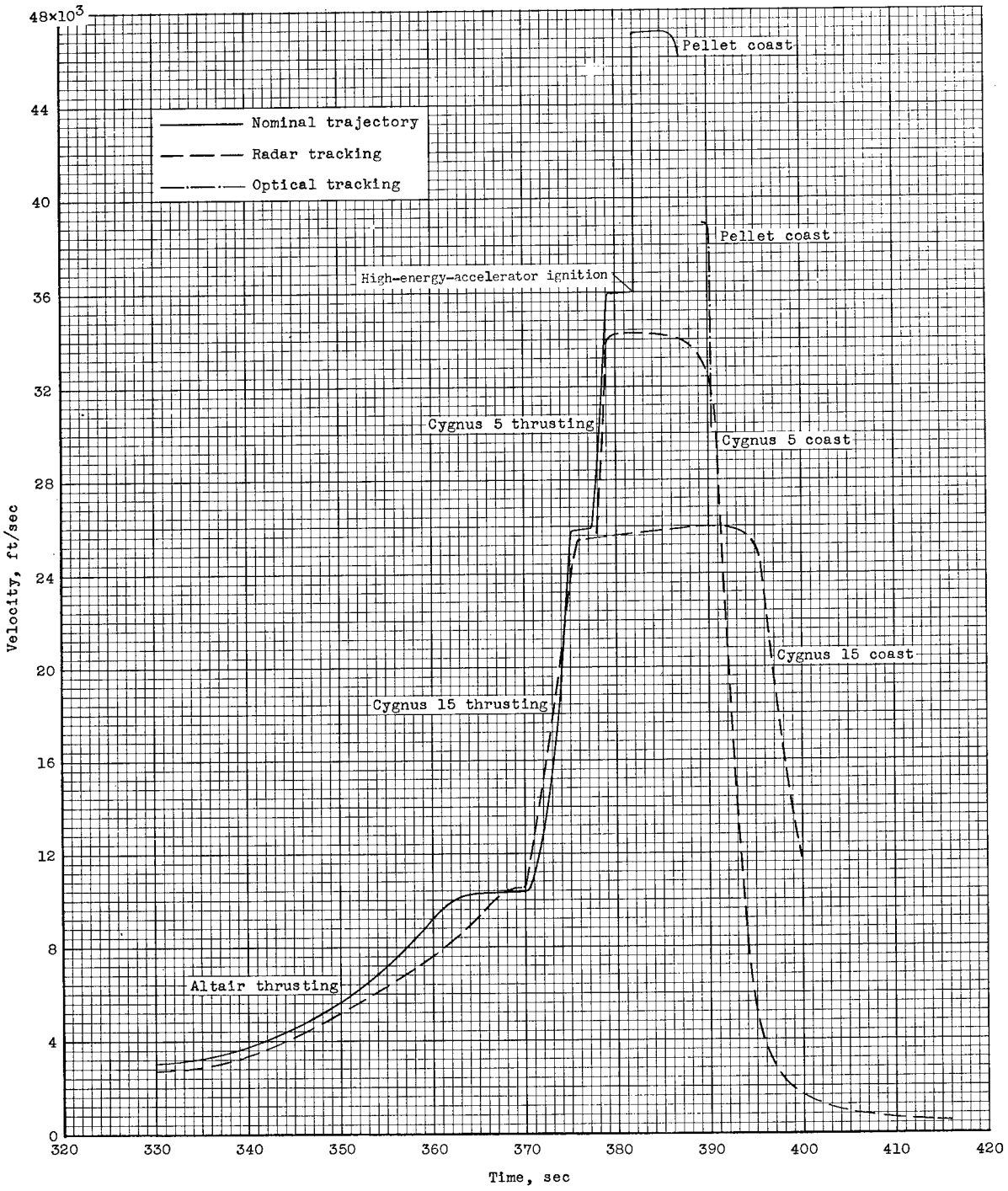

(b) Trailblazer IIb.

Figure 17.- Continued.

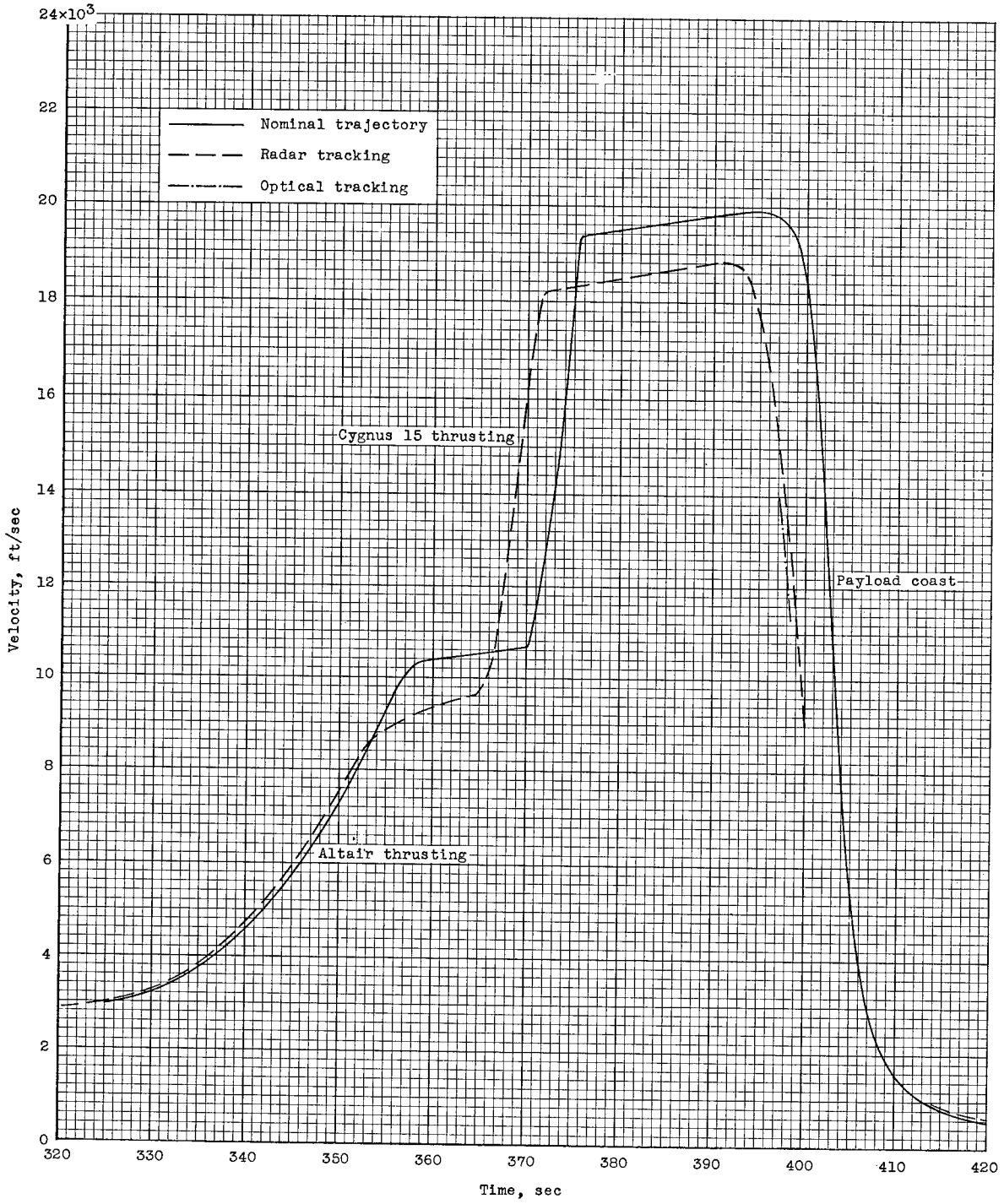

(c) Trailblazer IId.

Figure 17.- Concluded.

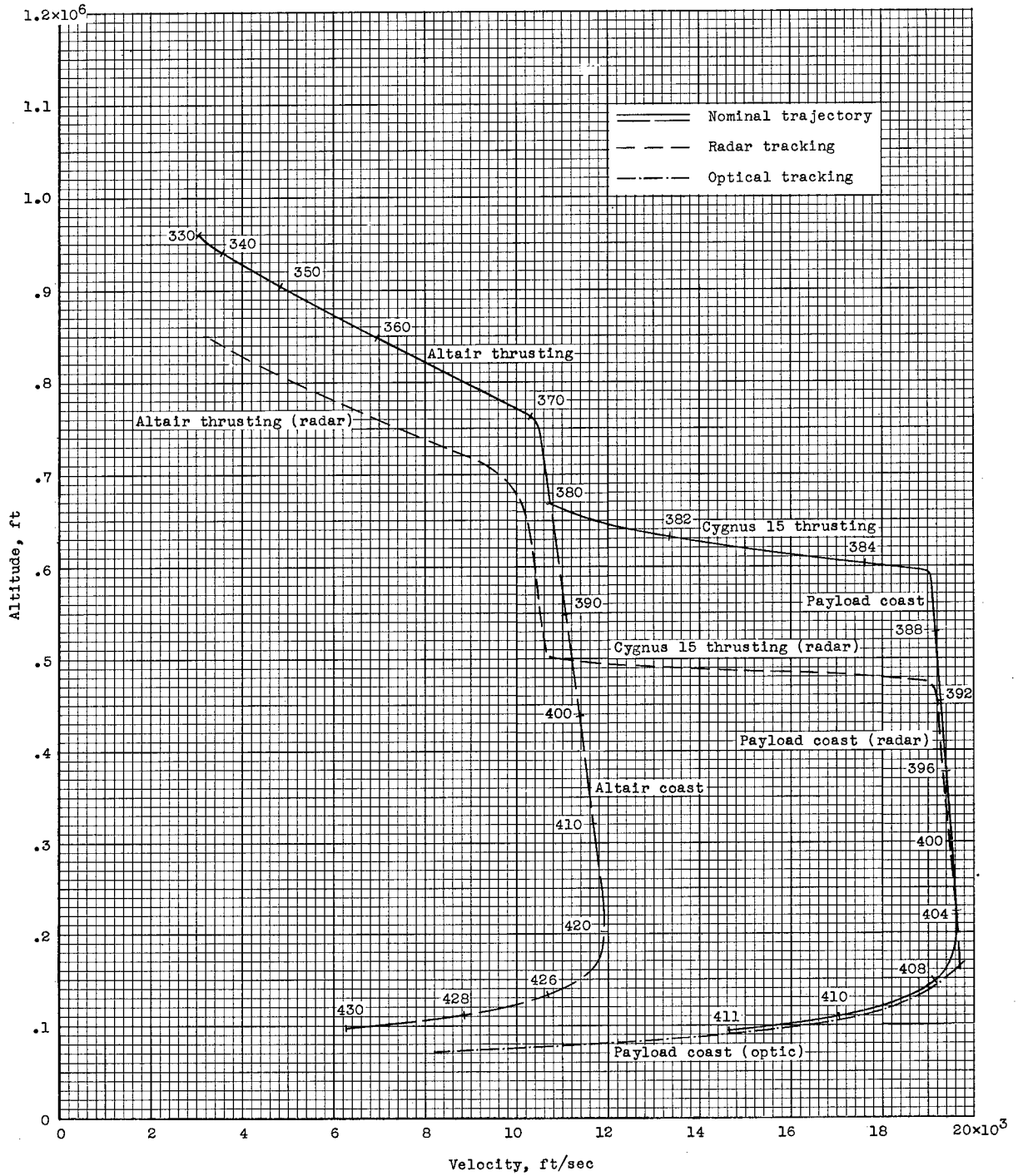

(a) Trailblazer IIa.

Figure 18.- Comparison of estimated altitude as a function of velocity for the reentry portion of the flight of three Trailblazer II vehicles with values obtained by radar and optical tracking. Ticks indicate time in seconds.

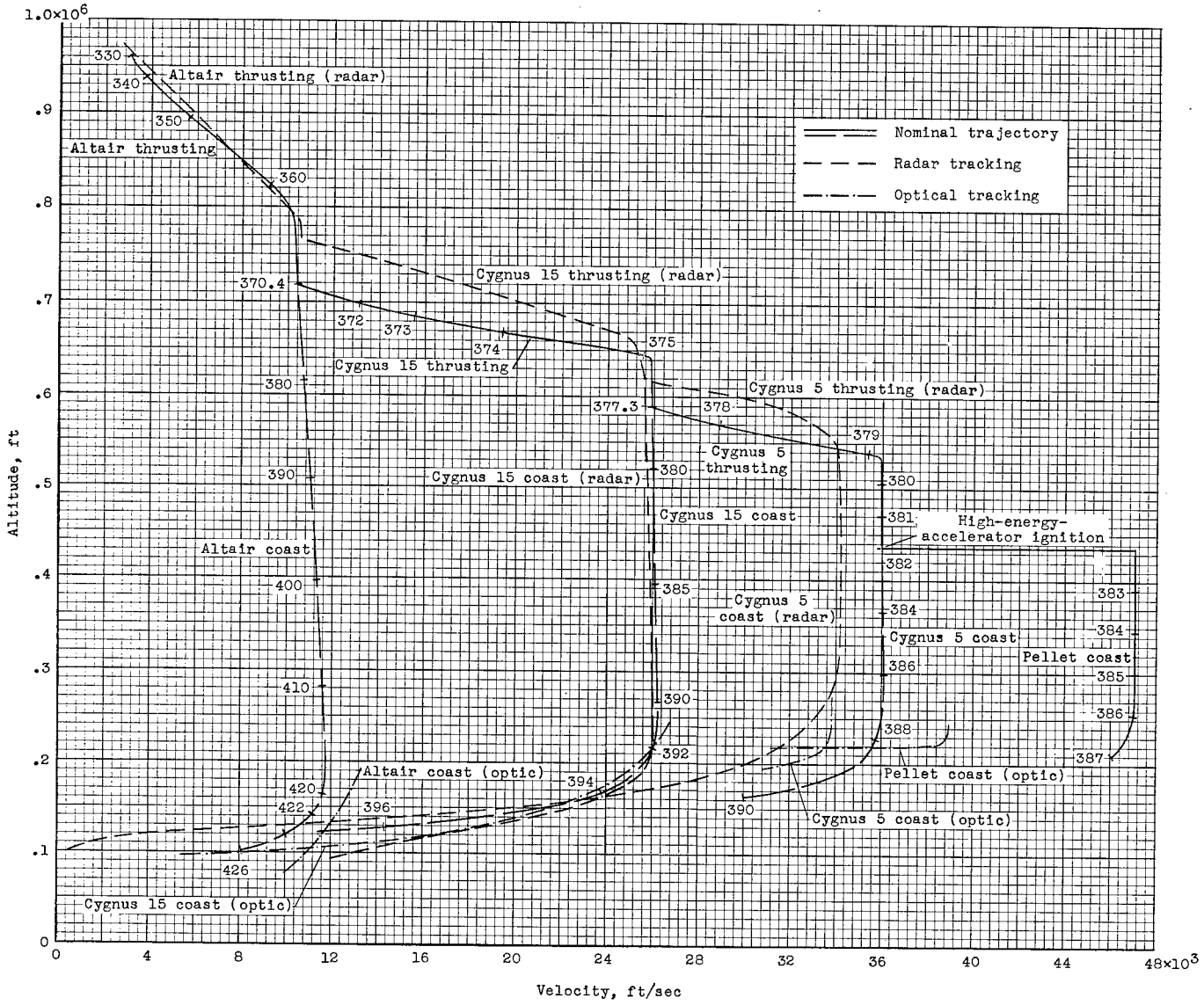

(b) Trailblazer IIb.

Figure 18.- Continued.

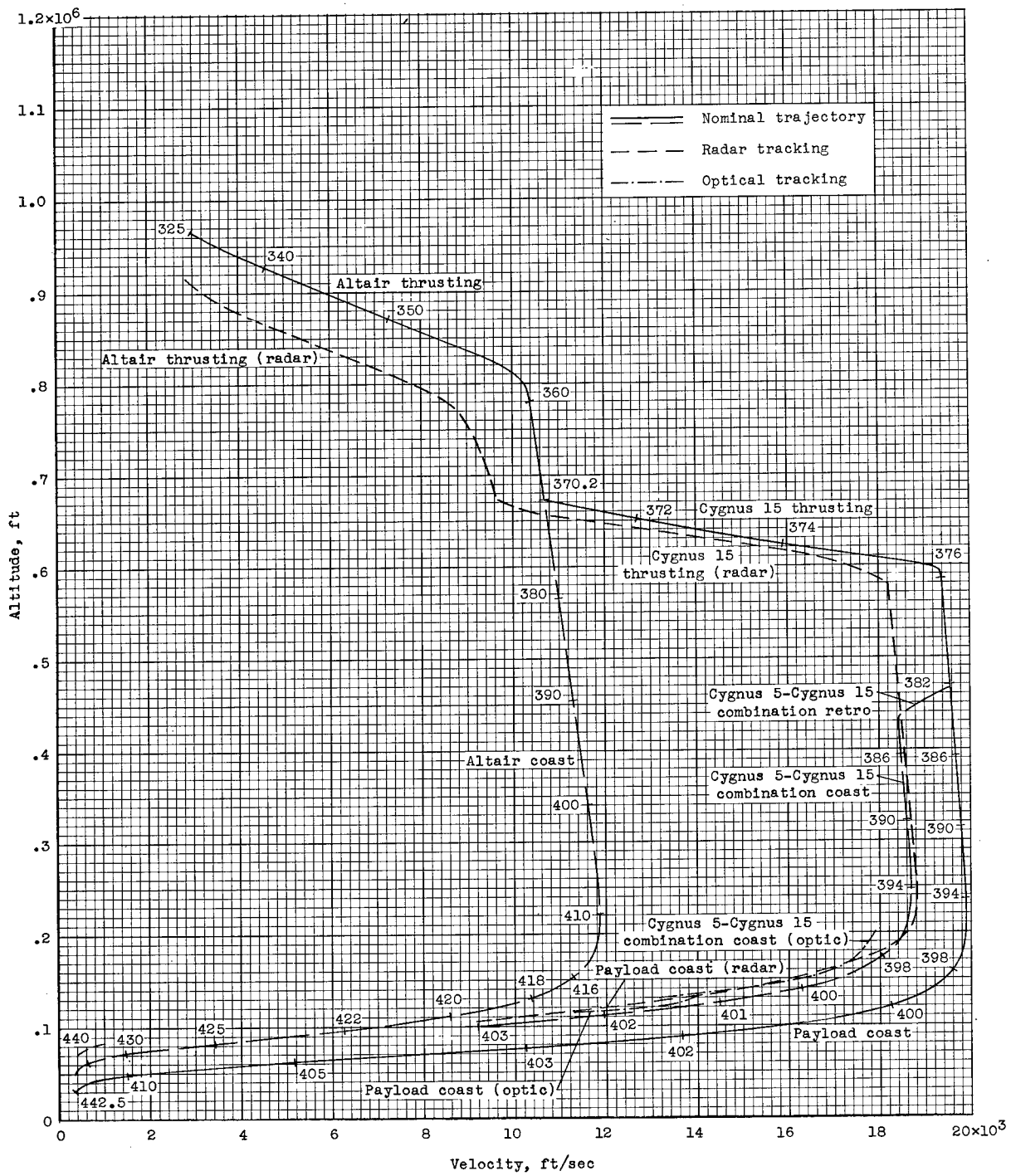

(c) Trailblazer IId.

Figure 18.- Concluded.

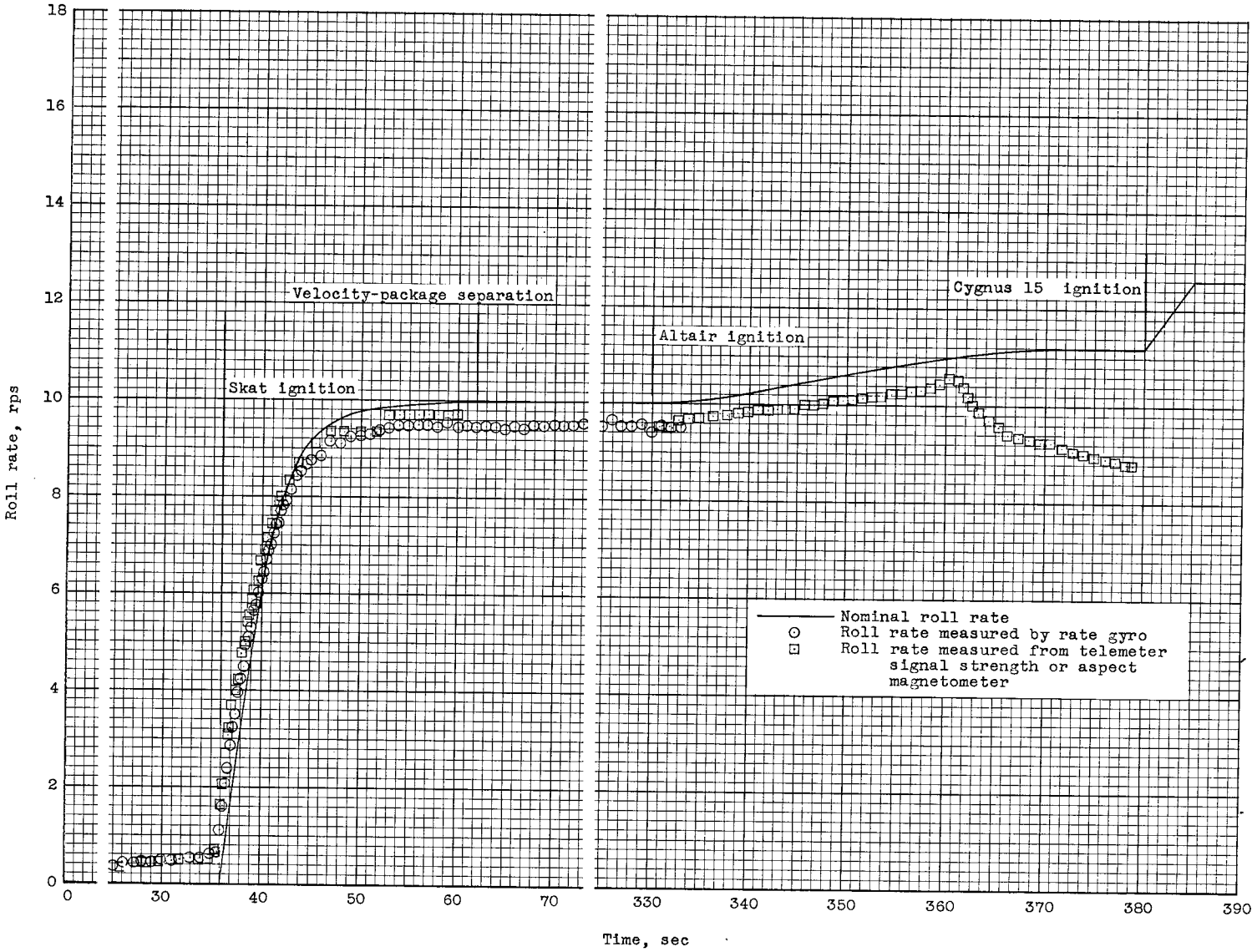

(a) Trailblazer IIa.

Figure 19.- Comparison of the predicted roll rate as a function of time for three Trailblazer II vehicles with values obtained from telemeter records.

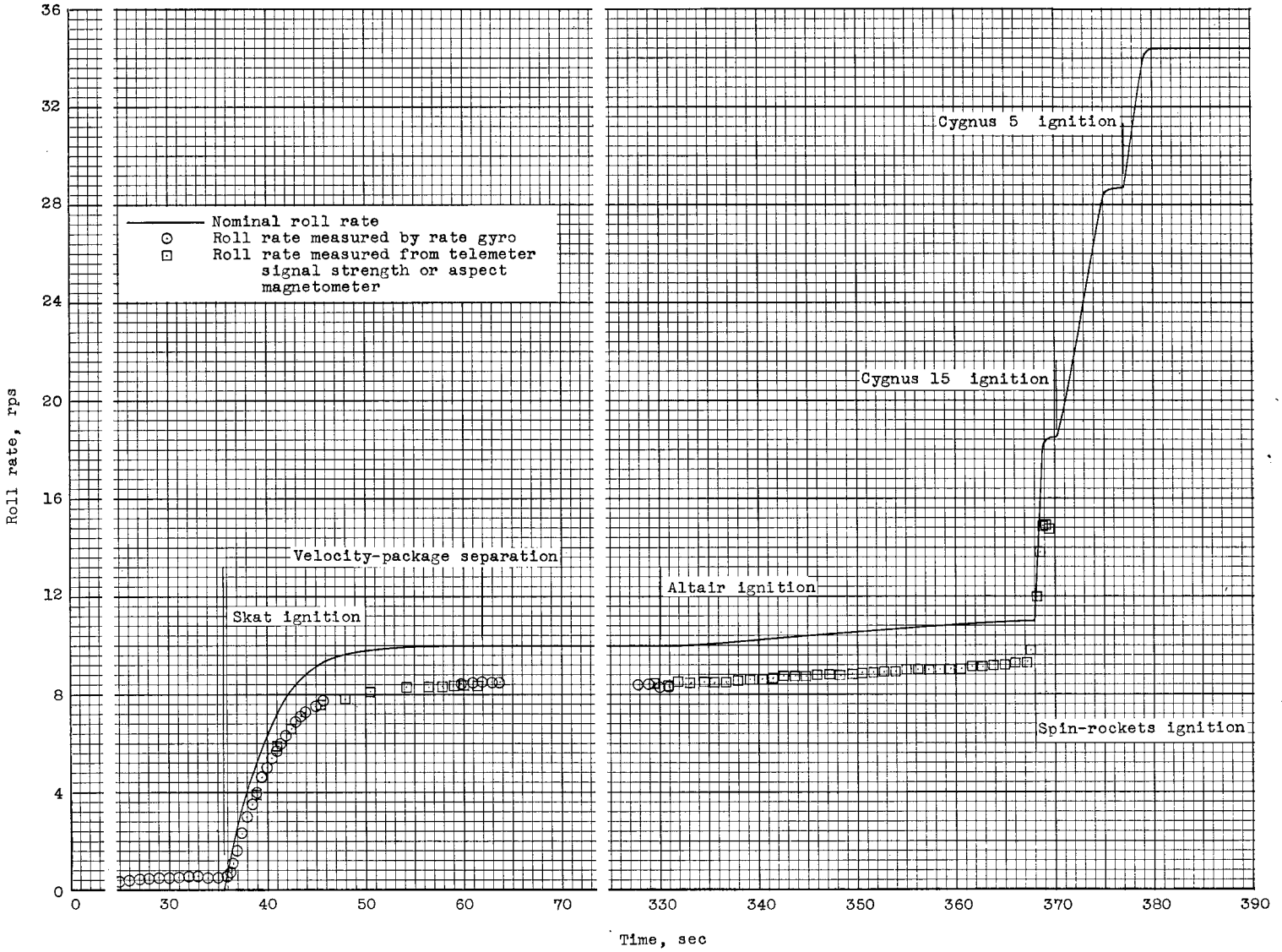

(b) Trailblazer IIb.

Figure 19.- Continued.

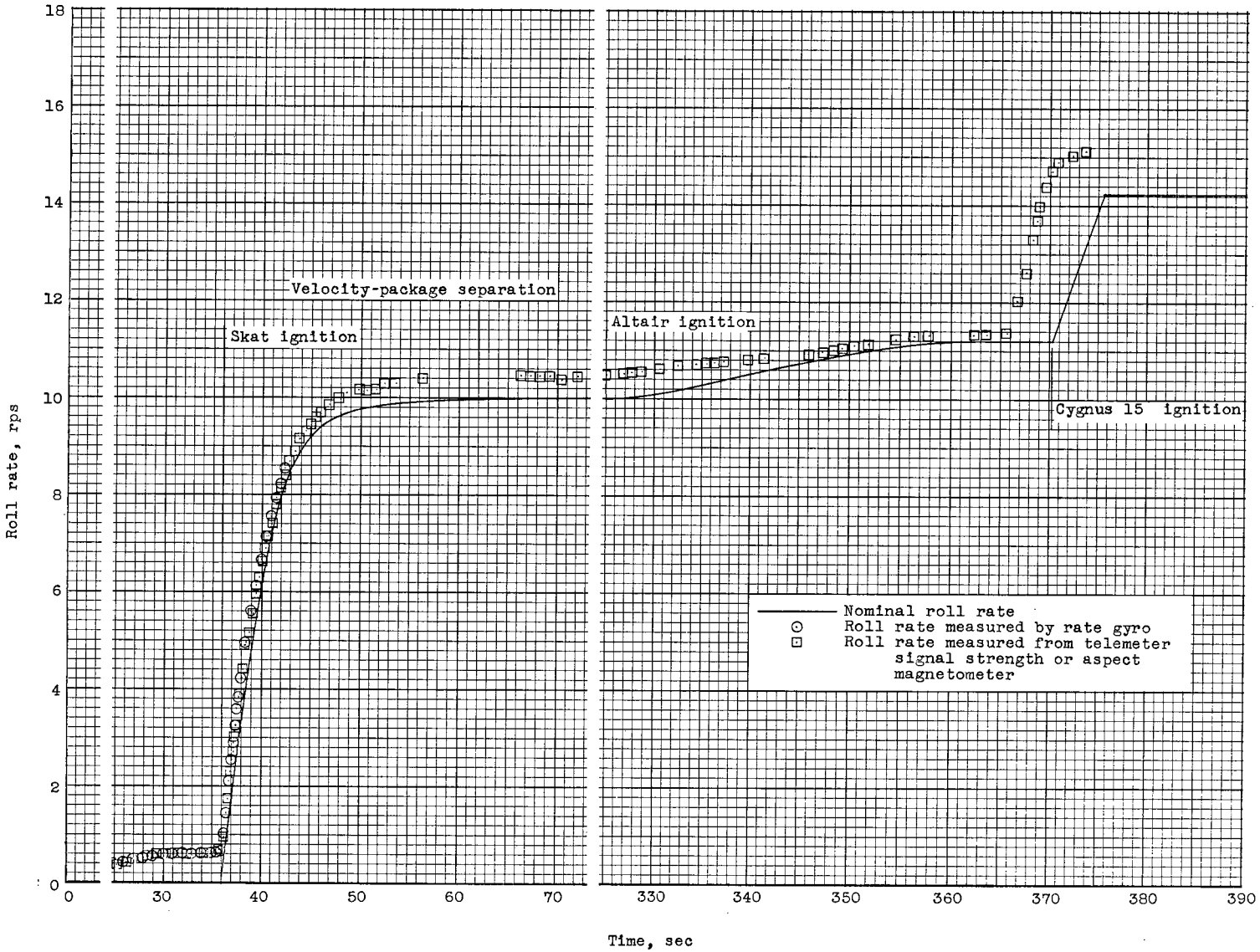

(c) Trailblazer IId.

Figure 19.- Concluded.

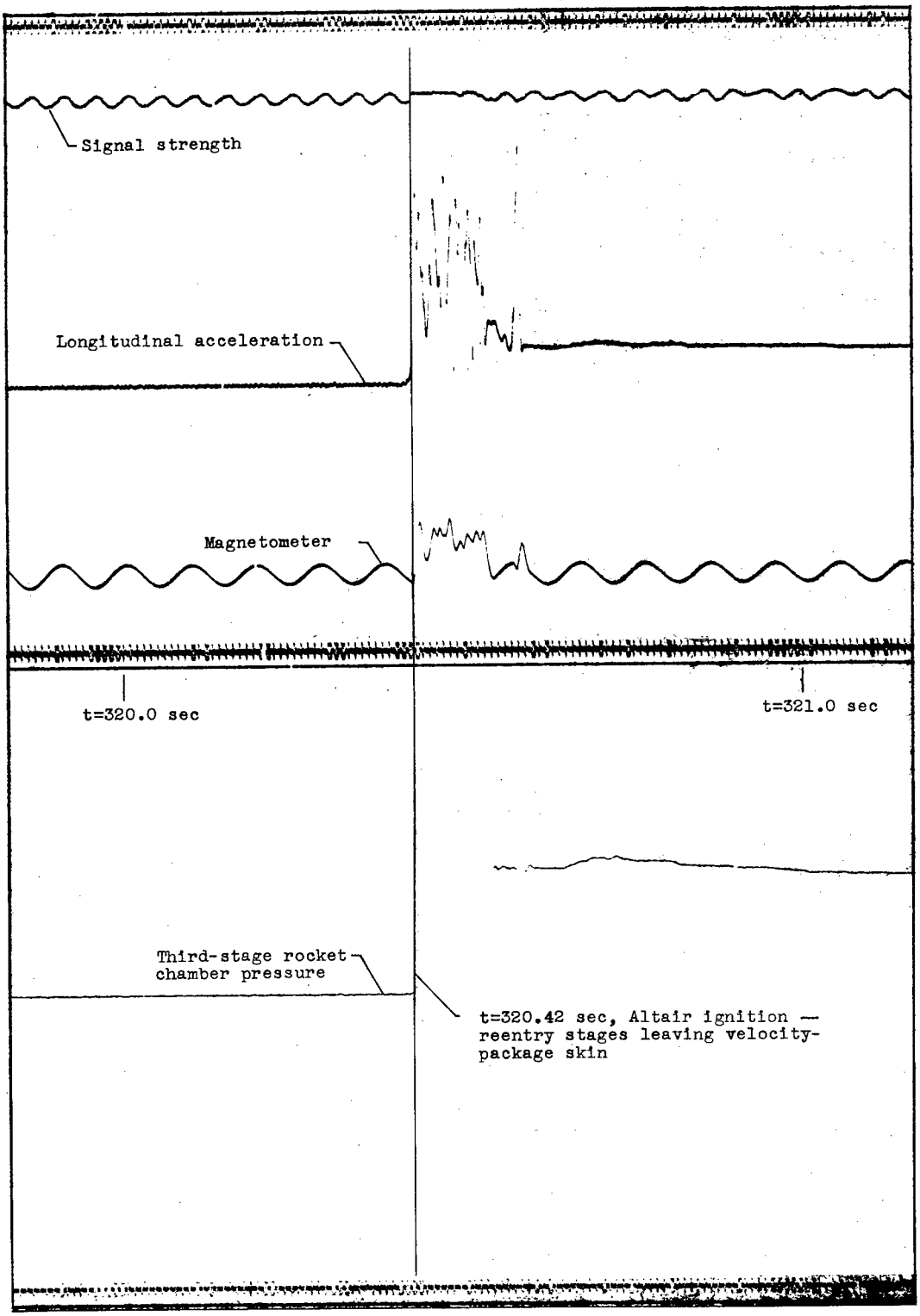

Figure 20.- Section of the telemeter record showing the Altair rocket-motor ignition from test flight of Trailblazer IId.

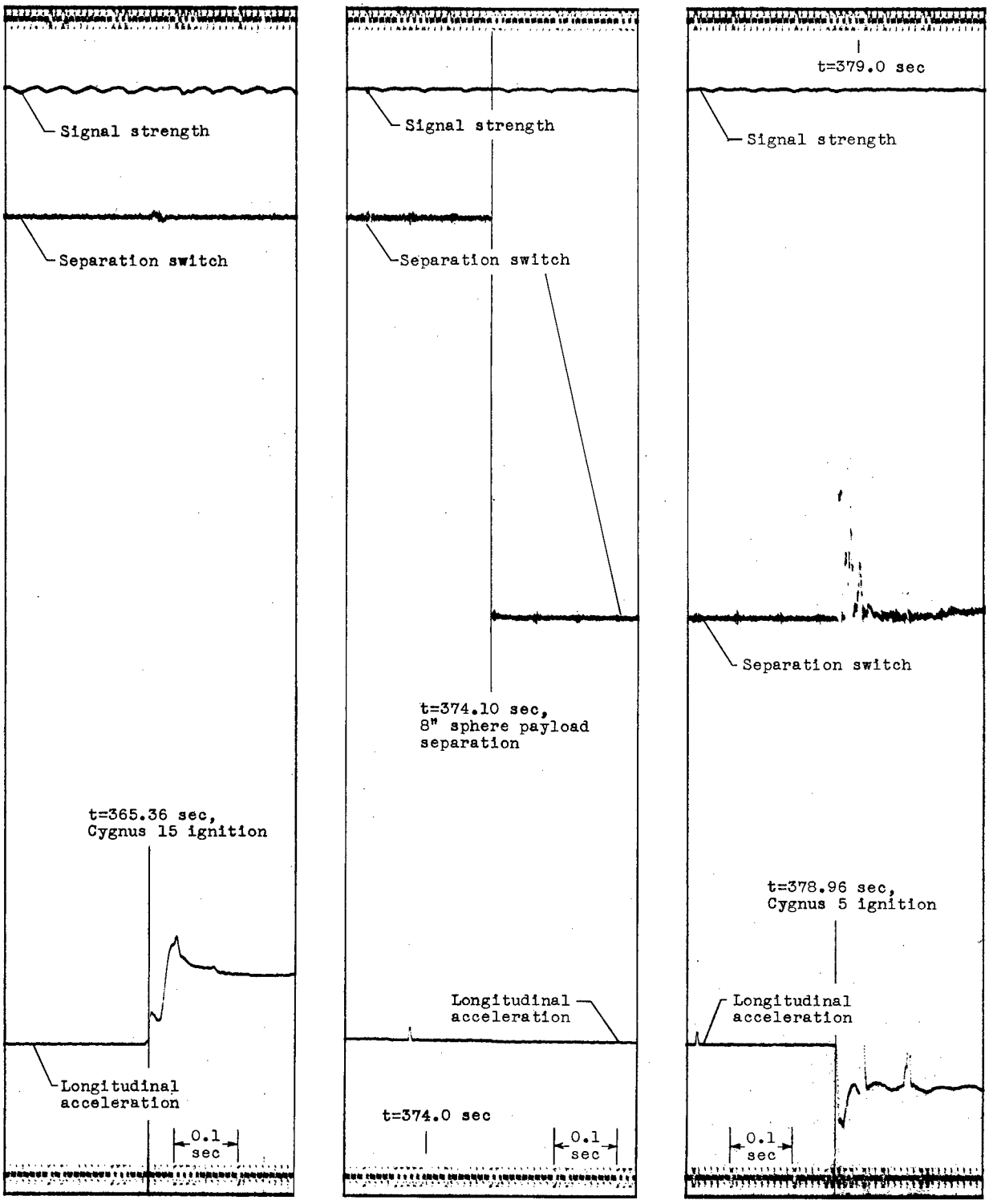

Figure 21.- Sections of the telemeter record showing Cygnus 15 rocket-motor ignition, payload separation, and Cygnus 5 retro-rocket-motor ignition from the test flight of Trailblazer IId.

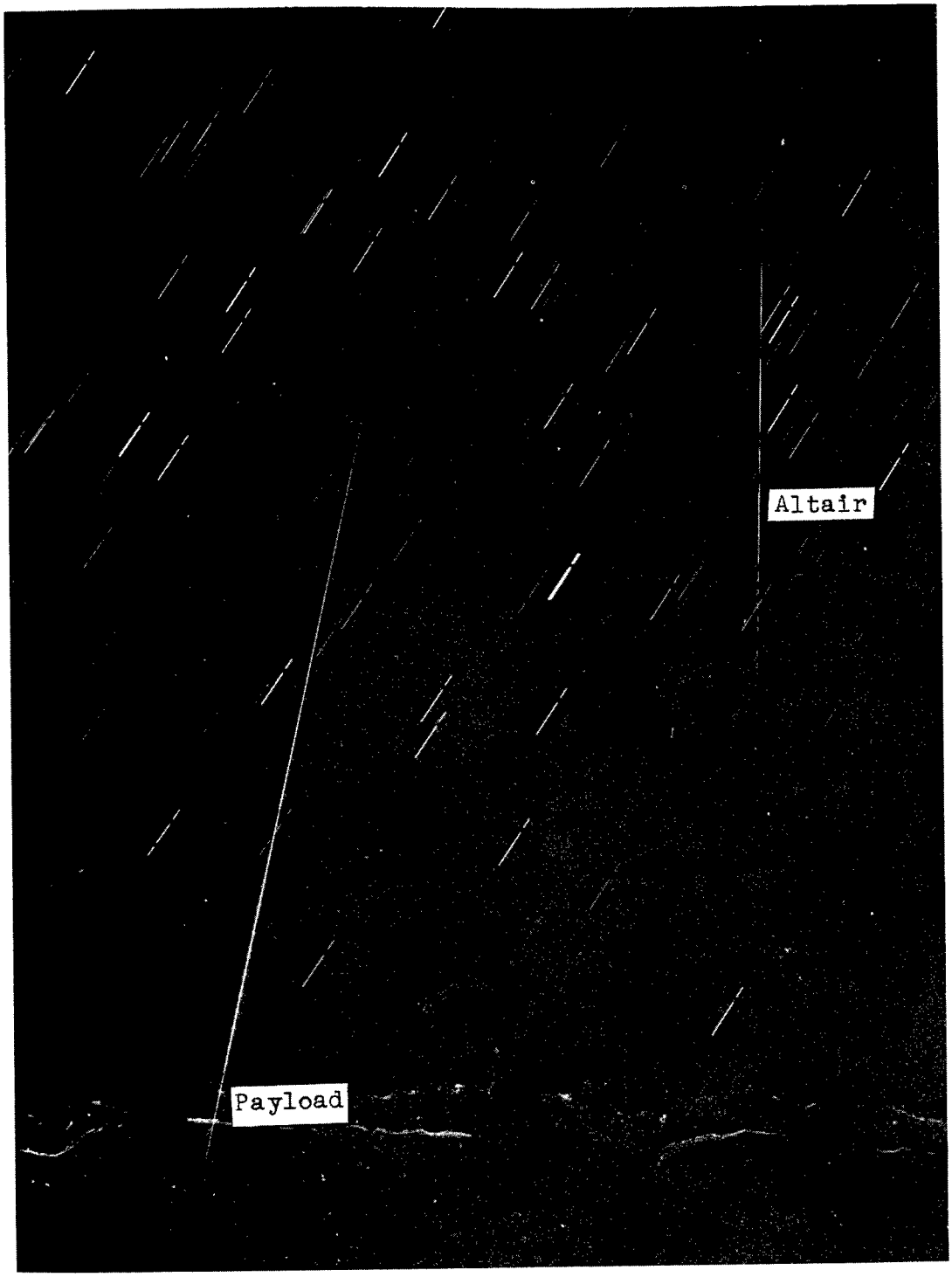

(a) Trailblazer IIa. L-64-4744

Figure 22.- Photographs of the reentry taken from Coquina Beach, N.C.

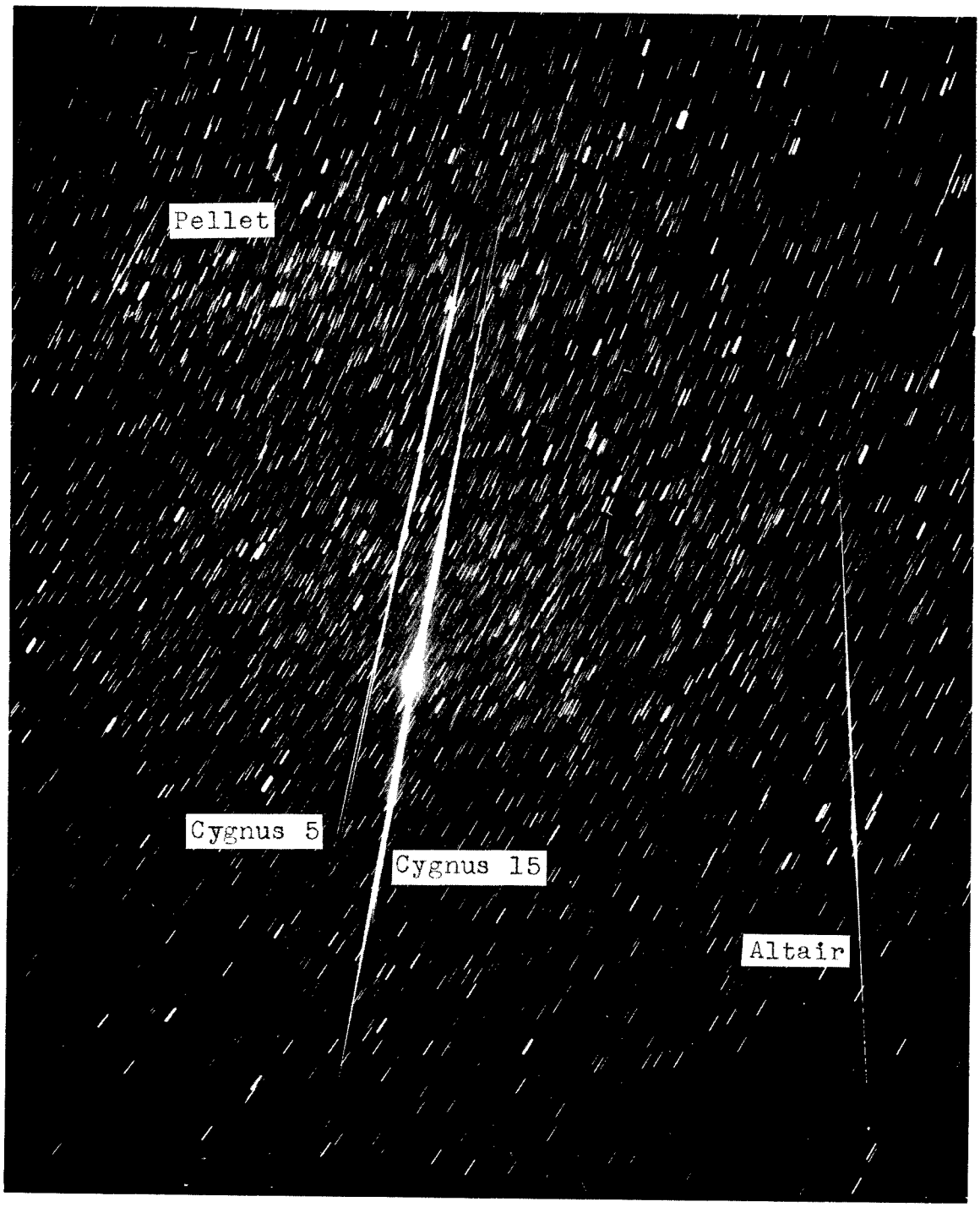

(b) Trailblazer IIb.

L-64-4745

Figure 22.- Continued.

(c) Trailblazer IId. L-64-4746

Figure 22.- Concluded.

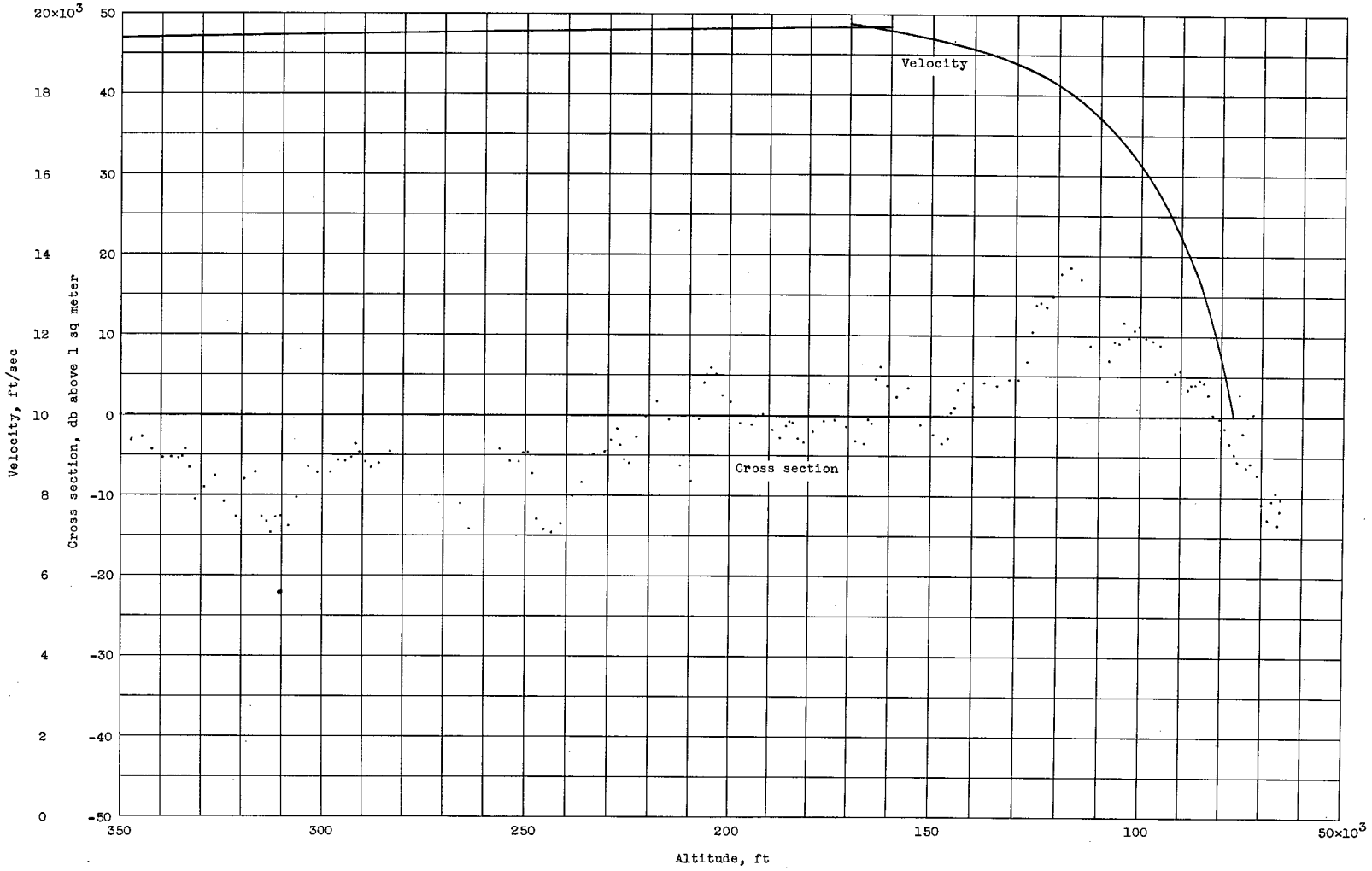

(a) Trailblazer IIa, S-band radar.

Figure 23.- Variation of radar cross section and velocity with altitude.

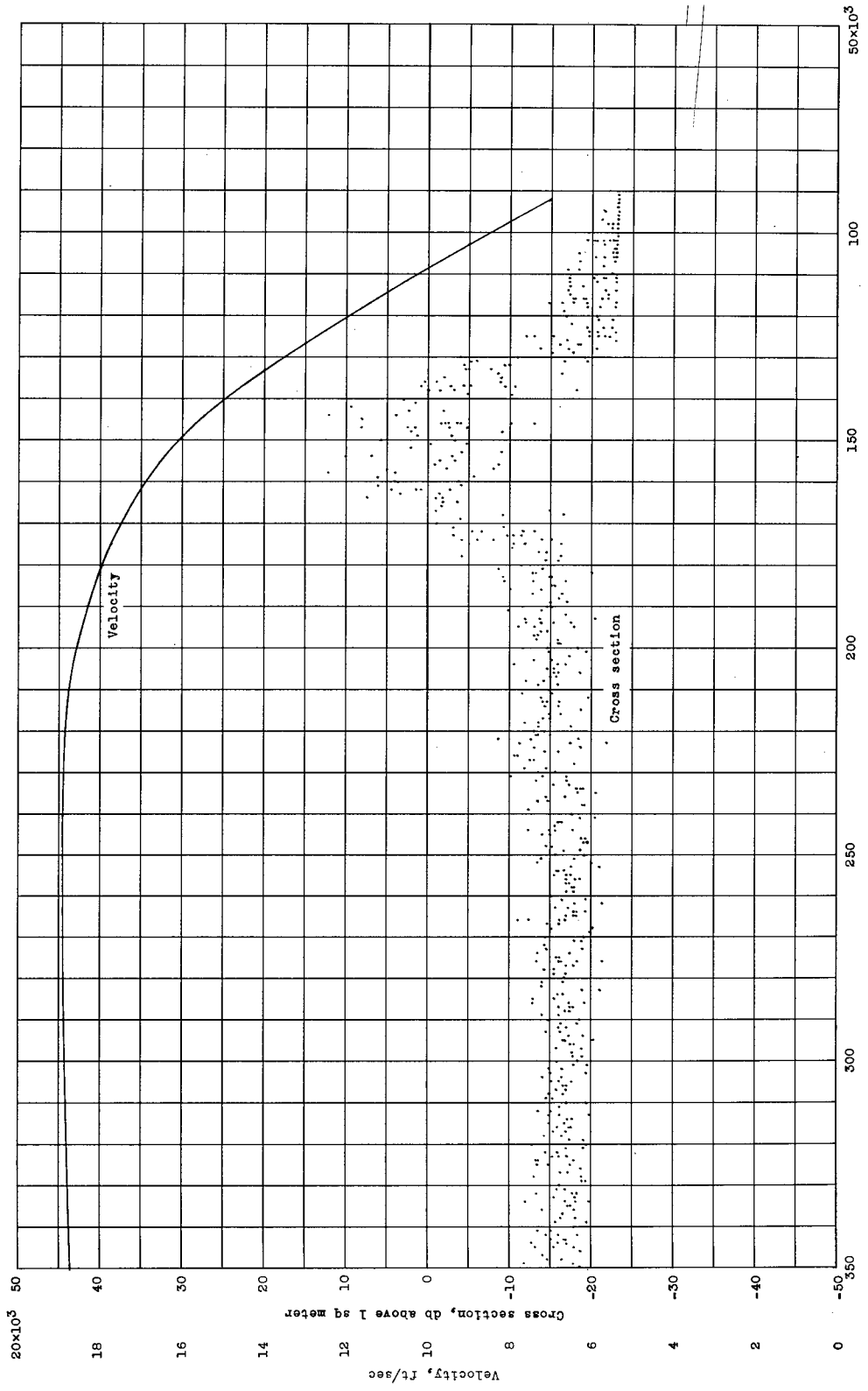

(b) Trailblazer IId, S-band radar.

Figure 23.- Concluded.

NASA TN D-1866
National Aeronautics and Space Administration.
DESCRIPTION AND PERFORMANCE OF THREE TRAILBLAZER II REENTRY RESEARCH VEHICLES.
Reginald R. Lundstrom, Allen B. Henning, and W. Ray Hook. December 1964. 61p. OTS price, $1.75. (NASA TECHNICAL NOTE D-1866)

The vehicle proved to be a workable system during flight tests by accomplishing its objective of reentering a prescribed payload at a high velocity near the predicted point of reentry. Wobble motions of the spinning body at various times were determined from the telemetered quantities. Pressure curves of the third-stage rocket motor and a thrust curve of the fourth-stage rocket motor under spinning conditions are presented.

I. Lundstrom, Reginald R.
II. Henning, Allen B.
III. Hook, W. Ray
IV. NASA TN D-1866

NASA

NASA TN D-1866
National Aeronautics and Space Administration.
DESCRIPTION AND PERFORMANCE OF THREE TRAILBLAZER II REENTRY RESEARCH VEHICLES.
Reginald R. Lundstrom, Allen B. Henning, and W. Ray Hook. December 1964. 61p. OTS price, $1.75. (NASA TECHNICAL NOTE D-1866)

The vehicle proved to be a workable system during flight tests by accomplishing its objective of reentering a prescribed payload at a high velocity near the predicted point of reentry. Wobble motions of the spinning body at various times were determined from the telemetered quantities. Pressure curves of the third-stage rocket motor and a thrust curve of the fourth-stage rocket motor under spinning conditions are presented.

I. Lundstrom, Reginald R.
II. Henning, Allen B.
III. Hook, W. Ray
IV. NASA TN D-1866

NASA

NASA TN D-1866
National Aeronautics and Space Administration.
DESCRIPTION AND PERFORMANCE OF THREE TRAILBLAZER II REENTRY RESEARCH VEHICLES.
Reginald R. Lundstrom, Allen B. Henning, and W. Ray Hook. December 1964. 61p. OTS price, $1.75. (NASA TECHNICAL NOTE D-1866)

The vehicle proved to be a workable system during flight tests by accomplishing its objective of reentering a prescribed payload at a high velocity near the predicted point of reentry. Wobble motions of the spinning body at various times were determined from the telemetered quantities. Pressure curves of the third-stage rocket motor and a thrust curve of the fourth-stage rocket motor under spinning conditions are presented.

I. Lundstrom, Reginald R.
II. Henning, Allen B.
III. Hook, W. Ray
IV. NASA TN D-1866

NASA

NASA TN D-1866
National Aeronautics and Space Administration.
DESCRIPTION AND PERFORMANCE OF THREE TRAILBLAZER II REENTRY RESEARCH VEHICLES.
Reginald R. Lundstrom, Allen B. Henning, and W. Ray Hook. December 1964. 61p. OTS price, $1.75. (NASA TECHNICAL NOTE D-1866)

The vehicle proved to be a workable system during flight tests by accomplishing its objective of reentering a prescribed payload at a high velocity near the predicted point of reentry. Wobble motions of the spinning body at various times were determined from the telemetered quantities. Pressure curves of the third-stage rocket motor and a thrust curve of the fourth-stage rocket motor under spinning conditions are presented.

I. Lundstrom, Reginald R.
II. Henning, Allen B.
III. Hook, W. Ray
IV. NASA TN D-1866

NASA

"The aeronautical and space activities of the United States shall be conducted so as to contribute . . . to the expansion of human knowledge of phenomena in the atmosphere and space. The Administration shall provide for the widest practicable and appropriate dissemination of information concerning its activities and the results thereof."

—NATIONAL AERONAUTICS AND SPACE ACT OF 1958

NASA SCIENTIFIC AND TECHNICAL PUBLICATIONS

TECHNICAL REPORTS: Scientific and technical information considered important, complete, and a lasting contribution to existing knowledge.

TECHNICAL NOTES: Information less broad in scope but nevertheless of importance as a contribution to existing knowledge.

TECHNICAL MEMORANDUMS: Information receiving limited distribution because of preliminary data, security classification, or other reasons.

CONTRACTOR REPORTS: Technical information generated in connection with a NASA contract or grant and released under NASA auspices.

TECHNICAL TRANSLATIONS: Information published in a foreign language considered to merit NASA distribution in English.

TECHNICAL REPRINTS: Information derived from NASA activities and initially published in the form of journal articles.

SPECIAL PUBLICATIONS: Information derived from or of value to NASA activities but not necessarily reporting the results of individual NASA-programmed scientific efforts. Publications include conference proceedings, monographs, data compilations, handbooks, sourcebooks, and special bibliographies.

Details on the availability of these publications may be obtained from:

SCIENTIFIC AND TECHNICAL INFORMATION DIVISION

NATIONAL AERONAUTICS AND SPACE ADMINISTRATION

Washington, D.C. 20546